Time Series Radar Observations of a Growing Lava Dome

Wadge, G.[1], Macfarlane, D.G.[2], Odbert, H.M.[1], James, M.R [3], Hole, J.K[1], Ryan, G.[4], Bass,V.[5], De Angelis, S.[4], Pinkerton, H.[3], Robertson, D.A.[2], Loughlin, S.C [4,6]

1. Environmental Systems Science Centre, University of Reading, Reading, RG6 6AL, UK
2. School of Physics and Astronomy, University of St Andrews, St Andrews, KY16 9SS, UK
3. Lancaster Environment Centre, Lancaster University, Lancaster LA1 4YQ, UK
4. British Geological Survey/Montserrat Volcano Observatory, Flemings, Montserrat, West Indies
5. Montserrat Volcano Observatory, Flemings, Montserrat, West Indies
6. British Geological Survey, West Mains Road, Edinburgh, EH9 3LA

To be submitted to J. Geophysical Research

Abstract

Exogenous growth of Peléean lava domes occurs by addition of lava from a central summit vent and mass wasting on the flanks as rockfalls and pyroclastic flows, forming an apron of talus. We observed this process at the Soufrière Hills Volcano, Montserrat between 30 March and 10 April 2006 using a ground-based imaging mm-wave radar, AVTIS, to measure the shape of the dome surface. From a time series of range and intensity measurements at a distance of six kilometres we measured the topographic evolution of the lava dome. The locus of talus deposition moved to the southeast with time and the talus surface grew upwards on average at about 2 m/day. The AVTIS measurements show an acceleration in lava extrusion rate on 5 April, with a 2-day lag in the equivalent rockfall seismicity record. We account for the budget of lava addition and dispersal during the eleven days of measurements using: AVTIS range measurements to measure the talus growth (7.2 Mm^3, 67%), AVTIS range and intensity measurements to measure the summit lava growth (1.7 Mm^3, 16%), and rockfall seismicity and visual observations to measure the pyroclastic flow deposits (1.8 Mm^3, 17%). This gives an overall dense rock equivalent extrusion rate of about 9.7 m^3s^{-1}. These figures demonstrate how efficient non-explosive lava dome growth can be in generating large volumes of primary clastic deposits, and how this process could also reduce the propensity for large hazardous pyroclastic flows.

1. Introduction

Lava domes are large rock masses that form complex, changing shapes as they grow by addition of magma from below. They are intrinsically unstable, forming talus slopes from rockfall mass wasting and generating pyroclastic flows from larger episodes of gravitational collapse that expose pressurized lava to the atmosphere. Such collapses tend to occur where new lava is added to the surface, a process that is important from the perspective of hazard evaluation [*Calder et al*., 2002]. Also the rate at which the dome grows is of similar significance, because of the potential to grow a hotter, more pressurized interior that may be more liable to explosive disintegration. The measurement of shape, locus of growth and lava extrusion rate are all of critical importance to understanding the process of lava dome growth and the hazards posed.

However, such measurements are often thwarted by the lack of close access, cloud cover and darkness. Opportunistic measurements by optical instruments (e.g. lidar surveys of the Mt. St. Helens lava dome, *Vaughan et al*. [2005], and Soufrière Hills Volcano, *Jones* [2006]) cannot capture the dynamics of growth as can a continuous time series of observations. In this paper we describe the deployment of a ground-based instrument: AVTIS (All-weather Volcano Topographic Imaging Sensor) to make such observations. AVTIS is a mm-wave dual-mode radar/radiometer (radarometer) instrument [*Macfarlane and Robertson*, 2004] that can image the range to, and temperature of, the surface of a volcano through cloud. Its technical capabilities are summarised in Table 1. AVTIS has been used to record the topography of a volcano [*Wadge et al*., 2004], to measure the advance of a lava flow [*Macfarlane et al*., 2005], and to estimate the extrusion rate and temperature of a lava dome [*Wadge et al.,* 2006]. During a two-week field campaign in March-April 2006, we used AVTIS to measure the growing lava dome at Soufrière Hills Volcano, Montserrat from two main sites at a distance of about 6 km. The range measurements made by AVTIS are quite distinct from the Doppler radar measurements made, for example, at the Merapi Volcano lava dome by *Hort et al*. [2006]. Those Doppler measurements were of the velocity of rockfall in the radar line-of-sight (LOS) and do not provide an image of the topography of the dome. After a discussion of the observational and measurement constraints, we present the time series of AVTIS data from both sites, together with the contemporaneous rockfall seismicity data that were gathered by Montserrat Volcano Observatory (MVO). We analyse and interpret these results in terms of the growth dynamics of the dome and talus.

2. Observational Context of the Lava Dome

The current eruption of Soufrière Hills Volcano began in 1995, and has produced a series of Peléean lava domes of andesitic composition within a crater (English's Crater) open to the east northeast [*Watts et al*., 2002] (Fig.1). These domes have been destroyed by collapse and explosion, usually producing pyroclastic flows, and re-grown repeatedly during three episodes of lava extrusion (1995-1998; 1999-2003; 2005-2007). Six weeks

after the field campaign reported here, the lava dome was destroyed on 20 May 2006, with most of the material being deposited in the sea to the east.

The lava domes at Soufrière Hills Volcano are fed by lava issuing from a central conduit within the crater. During the early stages of development, the lava dome typically grows as a contiguous flowing mass. Such endogenous growth is later replaced by exogenous additions of lava at the surface via shear-bounded surfaces through the earlier lava mass. This type of shear lobe mode of growth [*Watts et al*., 2002] can switch its locus of extrusion from one side of the dome to another. Surrounding the lava core of the dome is an apron of talus at an angle of repose of about 40º, derived from disintegration of blocks of lava from the top of the dome. This talus forms an increasingly large proportion of the whole dome as it grows. There are two main surficial processes that result in morphological change of the exogenous lava dome: addition of lava as contiguous masses or large (~10 m) blocks at the top of the dome, and the fragmentation of this lava to produce talus by rockfall and pyroclastic flow deposits.

At times during the ongoing twelve-year eruption, the dome at Soufrière Hills has grown up to 1000 m in diameter and up to 400-450 m high. The elevation of the crater floor at the conduit vent is about 700 m above sea level (asl) and the rim of the crater is at about 800 m asl. The elevations of both the crater floor and the northeastern crater rim fall towards the sea to the east northeast. As the dome grows within the crater, any pyroclastic flows and talus are constrained by the crater walls until the summit of the dome reaches an elevation of about 960 m asl [*Wadge*, 2007]. Above this, talus can spill out over the crater rim. At the time of the observations reported here the summit of the dome was at an elevation of 900-950 m asl and the talus was still contained within the crater (Fig.2).

We used AVTIS at two main sites on the eastern side of the volcano, Jack Boy Hill (JBH) and Runway, both about 6 km to the north northeast of the dome (Fig.1). The AVTIS lines-of-sight (LOS) thus covered the northeastern sector of the dome with the talus slope visible above the crater rim in the foreground (Fig.2). The direction of lava extrusion during the measurement period was to the east or southeast. Only part of the talus slope was visible from the two sites. So lava extruding near the summit of the dome tended to be pushed out and fall down slope in a dispersed fan of material, some of which became invisible to AVTIS if it moved out of view. Later we describe how we can take into account volumetric increases in talus that were not measured by AVTIS. We also deployed AVTIS at four other sites during this campaign (Fig.1, Table 2), but data from them are not discussed here directly.

3. AVTIS Measurements

The JBH and Runway sites were the closest (~6 km) practical, safe, vantage points for multiple occupation, but almost at the operational limit of the instrument (~7 km). At ranges of ~6 km, the signal-to-noise ratio (SNR) is low and discrete interference lines from the instrument electronics and motors can dominate the radar return signals of

interest. These discrete lines were removed prior to further processing. The reduction in return signal strength with distance reduced the accuracy with which the range to the surface can be retrieved. At ranges of ~3 km (as measured from St. George's Hill) the typical return signal from the volcano is about 12 dB above background (Fig.3) and has a SNR of about 2.5. Returned power is only about 2-3 dB above the noise level at distances of ~6 km (e.g. JBH) when the SNR falls to about 0.6. The result of a study that synthetically extended the range of the SNR values from these two sets of results is shown in Fig.3. The increase in the uncertainty of range values for single LOS is given by standard deviations that increase from about 4 m at a range of ~3 km to about 12.5 m at a range of ~ 6 km (Fig.3).

The spectrum of power received by AVTIS from the distant surface is quantized into 8192 bins, each bin representing 0.85 m of range. The instantaneous field of view of the radar, or footprint, on the volcano's surface is determined by the radar beamwidth, and the transverse resolution is ~52 m at a range of 6 km. However, in practice because the dome surface is not generally orthogonal to the radar LOS, the footprint will be larger and more irregular. Within a typical footprint on the dome the individual scatterers (e.g. lava block facets) will be distributed irregularly in range and will contribute variably to the strength of the return signal. Filtering of the radar signal to remove the effect of these localised scatters gives a better measurement of the range to the bulk topography [*Macfarlane and Robertson*, 2006], but at long ranges with low signal-to-noise the range bin chosen to represent the radar footprint can be dominated by the position of the largest surface facet most orthogonal to the radar LOS.

AVTIS takes about 0.25 s to send and receive the radar signal, process the data and move the radar to its next measurement position, and about 20 minutes to acquire a typical 100 by 50 pixel range image. Whilst the radar beamwidth is 0.5º, the angular stepping used in this study was 0.1º in both azimuth and elevation. This gave a considerable overlapping sampling of the surface that helped to reduce the noise in the resulting surface retrieval. The raster is built-up from the bottom of the image. Over the course of a typical 20 minute scan, a rockfall could have occurred that reduced the range to the top of the dome and would probably be measured, and increased it at the foot, but which may not be measured because the relevant part of the image had already been acquired, the incremental range change was too small to detect, or the deposit was below the field of view.

AVTIS does not have an internal means of measuring the absolute orientation of the radar beam. During this campaign the instrument was set up on a levelled tripod anew at each occupational epoch and the absolute position was measured using differential GPS. Absolute pointing knowledge was then acquired by the use of two tripod-mounted corner-cube reflectors placed at distances varying from a few hundred metres up to a couple of kilometres from the instrument and their positions also measured by differential GPS (Fig. 4). The reflectors were left in the field for the duration of the campaign. The known antenna pattern of AVTIS was then identified in the radar data giving the azimuth and elevation radar coordinates of both reflectors. Comparison with the GPS data then allowed the absolute orientation of the AVTIS pointing to be determined. These

measurements were performed before and after each AVTIS image acquisition so that the pointing coordinates could be averaged over each epoch. Analysis shows that the relative accuracy of angular referencing within each epoch is about 0.01º, reflecting the stability of the platform, the angular calibration, and the reproducibility of the radar pan and tilt gimbal. Between each occupational epoch (typically several hours of repeat measurements) the re-setting of the tripod means that the repeatability of the absolute pointing is much less.

The reflector measurements also acted as a correction for drift in the radar range measurement. The slope of the radar sweep which sets the received frequency to range conversion in the radar was found to drift slowly over the course of an epoch as the instrument changed temperature. After initial warm-up, the range accuracy would typically drift by up to 0.05% over the course of a single scan – i.e. a maximum drift of ~3 m at 6 km range, whereas over a complete epoch of several hours the range of drift could total as much as 0.5% (30 m at 6 km range). The GPS-measured reflector positions were therefore used to calibrate the range drift based on the apparent radar range at the start and end of each scan. This drift had not been noticed on previous AVTIS field campaigns since the range to terrain had previously been lower (typically 1 to 4 km) and repeat observations had only been at a range of 1200 m (implying a range drift less than the range resolution of the instrument).

3.1 LOS range accuracy with incidence angle

As the angle of incidence of the radar beam on the lava dome approaches a grazing angle at the dome margins, the footprint increases in size and the power returned falls, as forward scattering increases and the proportion of "sky" increases. Thus the margins of the dome where it is seen against sky, the "skyline", or against foreground or background surfaces will give weaker reflections and less accurate range measurements from AVTIS, particularly when signal-to-noise is already low.

We can evaluate this effect from the time series data themselves. On 2 April 2007, a series of fourteen range images of the dome was collected over a nine-hour period from Jack Boy Hill. The average surface generated from these data was taken as a reference and the local angle of that surface calculated to give an angle of incidence of the radar for each LOS. The variability of individual LOS range values among the fourteen individual scans from this surface was calculated for all angles of incidence from perpendicular (090º) to grazing (180º) (Fig. 5). In this case the average LOS was about +5º (upwards) from the horizontal and the average slope of the talus was +40º. Thus in Fig. 5 the incidence angle for the talus facing the instrument is about 155º. The standard deviation of the ranges is fairly constant at about 20 m until incidence angles of about 165º when it increases sharply. The effect of excluding data from the dome margins is to reduce the scatter throughout the inclination range (Fig. 5).

4. Time Series Results

4.1 Areal coverage

The JBH and Runway viewpoints reveal slightly different areas of the dome. The AVTIS data from Runway show more of the southeastern sector of the dome, but being lower in elevation than JBH more of the lowermost talus is obscured by the crater. The average area of the dome covered by AVTIS from both viewpoints is about 700,000 m^2, with a spatial density of range points of about 1 per 100 m^2. Due to instrument repositioning between epochs, no two occupational data sets are identical, but Fig. 6 shows the maximum areas covered from the two viewpoints. Both comprise about 50% lava surface in the southwest, far range, and 50% talus in the northeast, near range. The area of overlap of any pair of datasets can be several tens of percent less than the area of an individual image. Fig. 6 also shows that a sector of about 180° was thought to be actively involved in mass wasting during this period.

4.2 Combined range measurements

As we have discussed, individual AVTIS range measurements during this campaign were subject to inaccuracies arising from low signal strength, interference, drift, local scattering effects and pointing uncertainties. We reduced the resultant noise in the range data by temporal stacking of scattering spectra within each occupational epoch (Table 2), a step necessitated by the low signal-to-noise values of these data. The resultant average epoch range values were then combined with absolute orientation data in order to provide 3D coordinates of surface points that were then interpolated spatially onto a 10 m grid (Montserrat local grid coordinates) by kriging. Temporal stacking in this way means that any topographic changes during the period of the occupation will be averaged. The overlapping fields-of-view of the radar (each surface point contributing to as many as 25 (5 x 5) range values) reduces the uncertainties on the derived surface. However, at the "skyline" the benefits of this are reduced.

4.3 Surface differences

The occupation-averaged surfaces should represent the visible dome surfaces at the mid-point of each epoch. With accurate co-registration, the differences between surfaces should then represent the topographic changes to the dome during the relevant interval, often daily. Offsets in instrument orientation between occupations can be reduced by comparing surfaces retrieved from terrain known to be stable, away from the dome. In this case we used the outer, north-facing slopes of the volcano below the crater rim, at a range of about 5 to 5.5 km, only slightly less than that to the dome itself. Occupation-averaged surfaces of this terrain (an area of 0.1 km^2 and a slope of about 25°) show standard deviations of elevation of about ± 3 m, when adjusted to their optimum fits. On the dome, to avoid the effects of the noisier "skyline" data, some of these data points were masked prior to surface differencing, mostly those in the elevation range 870 to 910 m asl.

Figs. 7 and 8 show the surface differences for each successive occupation for JBH (relative to 2 April 2006) and Runway (relative to 30 March 2006) sites respectively and Table 4 gives the net volumetric changes and areas of overlap used to calculate those

changes. With two exceptions, successive differences show net increases in volume. From Runway, the uppermost southeastern part of the dome shows a large negative area developing between 30 and 31 March. Five days later on 5 April, the negative feature is reduced in magnitude and area and a large positive feature has formed immediately to the east. In the succeeding two days (6 and 7 April) this trend continues. We interpret the negative feature to be result of a large collapse event, removing 40 m or more of dome and moving it out of the measurement area.

There were no equivalent measurements from JBH on 30 and 31 March, and the coverage from JBH includes only the northernmost parts of the two main features measured from Runway. A distinct negative feature can be seen in the JBH data on the south central part of the dome (Fig. 8). Like the Runway data most of the new talus volume is added to the lowermost eastern slopes. There was a negligible change in measured talus volume between 8 and 9 April. As we shall see, this was a period of increased pyroclastic flow activity and it may be that this low net volume was because the rockfall transport was particularly effective in moving it away from the upper talus slopes. The uncertainties on these estimates must be higher than those for the outer crater differences (± 3 m), mainly because of "skyline" error. They have not been independently quantified and an uncertainty level of ± 5 m is assumed.

The average rate of increase of the surface (Table 4) is about 2.0 m/day; 14 ± 5 m over 7 days for JBH, and 17 ± 5 m over 8 days for Runway. The volumetric rate of addition for these two intervals is 1.4 m^3s^{-1} for JBH and 1.9 m^3s^{-1} for Runway. However, a considerable portion of the talus and the volume that must have accumulated there is hidden from both viewpoints. The profiles through the Runway surfaces for 30 March and 7 April (Fig.9) show these inferred hidden accumulations.

4.4 Intensity measurements and the elevation of the summit of the dome

The strength (intensity) of the signal received by AVTIS is a function of the range distance, path attenuation, the local scattering and dielectric properties of the surface (reflectivity), and the angle that the surface makes with the radar beam. Typically, the variability of the intensity across the dome's surface is about 3-4 dB at a range of 6-7 km. *Macfarlane et al*. [2006] were able to distinguish the highly reflective surfaces of new lava flows from less reflective ash-covered surfaces at a distance of about 3 km using AVTIS intensity images of Arenal volcano. No such ready distinction is apparent at Soufrière Hills, where the talus and lava surfaces tend to exhibit similar intensities. Fortuitously- oriented blocks of lava do often give stronger intensities than their surroundings and the continuity of some of these can be tracked in the time series over several days.

The skyline of the dome viewed by AVTIS from Jack Boy Hill or Runway has a diminishing intensity as increasing amounts of "sky" dilute the return signal from the dome (section 3.1). Nevertheless, the AVTIS-derived profile does yield useful information about the elevation of the summit of the dome and from that the component of the lava output that remains as part of the dome core. Fig. 10 shows a pair of intensity images from both measurement sites. Over the eight-day and seven-day intervals

separating the images in the two pairs obvious major changes have occurred. The elevation of the more easterly of the two peaks has grown and the gradient of the more southeasterly profile (to the left of each image) has reduced slightly with time. From such images, the equivalent elevations of the surfaces derived from the range data, and from photographs we have estimated the changing summit profiles with time. The highest parts of the dome measured by AVTIS from the daily surfaces are shown in Table 4. Given the inaccuracies of skyline measurements discussed earlier, these values are only reported to the nearest 10 m interval. Between 30 March and 6 April the dome increased its maximum elevation from about 910 to about 950 m asl. There seems to have been no further increase measured after that up to 9 April. On 18 May 2006 the elevation of the dome summit was surveyed by total station as 1006 m asl.

5. Rockfall and Talus

5.1 Mechanics of Rockfall

Rockfalls, and the avalanches they generate, are rapid movements of rock mass under gravity originating on steep slopes. The dimensions of the rockfall mass at source are largely defined by the jointing in the rock mass. The failure of a large mass (longest dimension > 10m) along a particular plane of weakness may be followed by the disintegration of that mass along joint planes. Individual rocks may bounce, slide or roll down the slope. They may also collide with each other and these events, if numerous enough, can generate a granular mass in a state of mechanical fluidisation. Experiments show that rocks at the front of such a mass are accelerated forwards as a result of this process, and rocks at the rear are decelerated [*Okura et al*., 2000]. This will result in a greater areal coverage of deposit than would be the case if the rocks fell individually. In addition, rock clasts may also fragment under shear stress, particularly at pressure and depth in the flow [*Davies et al*., 1999]. This fragmentation process will itself create an additional dispersive stress that, like the mechanical fluidisation process, will tend to cause the avalanche mass to inflate and spread.

Rockfall from active lava flows, as at Soufrière Hills, has the additional factor of gas contained within vesicles in the rock. This is believed to result in a propensity for autobrecciation. The release of pressurized gas fragments the lava surface leading to a sort of rapid exfoliation to produce ash. This has been observed at Soufrière Hills [*Calder et al*., 2002] and at other lava domes such as Unzen [*Sato et al*., 1992]. *Calder et al*. [2002] distinguished between "passively generated" rockfalls derived from the cold carapace of the dome and "actively generated" rockfalls derived from freshly extruded lava fronts. The former were seen as largely degassed, with runouts rarely extending beyond 500 m from the source, and with an upper volume of about 10^3 m^3, the latter as gas-rich and grading into small pyroclastic flows. Auto-fragmentation is therefore probably the dominant process in both the generation and mobility of pyroclastic density currents derived from lava dome collapse and also in the long runout character of large rockfall avalanches [*Davies et al*., 1999].

5.2 Talus Growth

From the above discussion we should expect that the talus adjacent to the lava dome has been derived from the "passively generated" rockfalls and to be relatively coarse grained. Although it has not been well studied, the talus at Soufrière Hills does have a significant proportion of finer grains. These may be derived from more gas-rich events whose main mass is deposited outside the talus but which leave a deposit of finer material in transit.
The slope of the talus varies between about 42º at the exposed core lava to about 33º at the distal edge of the talus, with an average of about 37º. It maintains a fairly constant profile as the dome grows. In March-April of 2006 the summit of the dome was at an elevation of over 900 m asl, about 200 m above the vent. Within English's Crater, the distal edge of the talus rested on a slope of about 13º to the east northeast, whilst to the north, south and west the talus was banked up against the crater walls. Because the sector of lava extrusion was on the eastern side of the dome at the time of the AVTIS measurements, it is this talus slope that is the focus of interest. In particular, we want to know how material is distributed on this talus slope from any given rockfall event at the dome.

Fig. 11 shows a geometrical model of the situation and we make the following simplifying assumptions. The dome and talus is represented as a right conical frustum on a conical base. The talus slope is θ and is maintained constant as the dome grows. The base is also a conical frustum with an upper slope of θ'. The upper and lower radii of the frustum are R_2 and R_1 respectively. R_2 is fixed (representing a fixed width of exposed dome). As the dome grows in height the outer radius of the talus increases. The volume of the dome and talus, V_{dt} , is given by:

$$V_{dt} = 1/3\ \pi\ (R_1 - R_2).(\tan\theta - \tan\theta').(R_1^2 + R_1R_2 + R_2^2) \quad , \qquad (1)$$

and the lateral (non-summit) surface area, A_{dt} , by:

$$A_{dt} = \pi\ (R_1 + R_2).(R_1 - R_2)/\cos\theta \quad . \qquad (2)$$

If a rockfall distributes its mass equally along the length of its runout whilst spreading over a sector set by the angle occupied by the mass at the dome, then the thickness of the resulting deposit will reduce considerably as it spreads, according to equation 2, by more than an order of magnitude, over the length scale appropriate for this case (Fig. 11). Conversely, for a constant thickness increment added to the talus, much more volume of material must be added at greater distances. For example, to achieve the 2 m/day incremental thickness addition to the talus measured by AVTIS, over a 180º sector with values appropriate for April 2006: R_2 = 100 m, R_1 = 500 m, θ = 37° and θ' = 13°, would require a volume of about 956,000 m^3 per day. The production rate of talus would be about 11 m^3s^{-1}.

In reality there will be many exceptions to this simple view. The deposits from individual rockfalls will form a topography that departs from this steady state at any give time. The slope of the lowermost talus will be less than average and mass with sufficient energy may tend to accumulate here. Also the infrequent, larger collapse will send pyroclastic flow material beyond the talus slope altogether. Nevertheless, the above geometrical model does give an approximate method of accounting for the volume budget.

5.3 Rockfall Seismicity

Montserrat Volcano Observatory (MVO) routinely records rockfall seismicity from its network of broadband seismometers and extracts the time, duration, repose intervals and energy release for each event. However, a large number of smaller volume rockfalls impart too little energy to the ground to be recorded as a network event. So the rockfall seismicity catalogue represents only the largest magnitude occurrences of all rockfalls. MVO distinguishes between rockfall (RF) and long-period rockfall (LPRF) events. RF events are characterised by high frequency spectra (2-8 Hz) and LPRF events have an additional spectral peak in the 1-2 Hz range. This long-period component originates from fluid resonance in the conduit and is sometimes associated with gas releasing into the atmosphere, particularly when the extrusion rate is fastest [*Luckett et al*., 2002]. *Luckett et al.* [2002] argued that, whilst there was no simple relationship between the rate of extrusion of lava and the rate of RF generation, there was a positive correlation with the rate of LPRF generation. *Calder et al*. [2005] showed that for rockfall data for the 1995-97 period, the duration of each event increased, and the repose intervals decreased, with increased extrusion rate of lava, particularly for higher rates. Data on repose intervals between rockfalls could be fitted to log-logistic survivor functions, suggesting that mechanisms promoting internal physical forcing to failure control the relationship.

The number of recorded RF and LPRF events during the AVTIS campaign increased at the start of the measurement period from a lower level, dipped on 5/6 April, and peaked on 8 April (Fig. 12). The proportionality of RF and LPRF events was nearly constant throughout the period (Fig. 12). The energy measured for each event varies with instrument and location. In the following, we have used mainly the MBGH seismometer, located about three km west of the dome. For part of 9 and 10 April we have also used the MBLY seismometer record, which was the only instrument operating during that interval. By calibrating MBLY against MBGH we have substituted the appropriately scaled MBLY data for 9/10 April into the MBGH record. Generally, the seismic energy released varied greatly over this period (Fig.13). Several large magnitude events occurred on 31 March and the largest single energy release in the period was from an event on 10 April. Some of these events were observed to correspond to the generation of pyroclastic flows. The period 5-7 April was notable for a lack of larger magnitude events.

6. Accounting for Dome Growth

6.1 Photographic and photogrammetric observations of the dome and talus

From photographs taken from the AVTIS measurement sites we know that the lava dome changed its shape and size during the AVTIS observation period. The summit of the

dome increased its elevation, at least one large dome block collapsed and the surface of talus increased its elevation. This talus growth occurred on the eastern side of the dome. Photographs from the Perches site (Fig. 14) on 23 March and 10 April show this clearly. Over that eighteen-day period, the talus increased its extent to the southeast, burying an area of fumarolic activity. When this lateral spreading of talus occurred is not certain, but the increased rate of rockfall and the large collapse events on 31 March makes this a likely contender for the start of this change. A rise in the general elevation of the talus can be seen in Fig.14, particularly along the retaining wall on the northeastern side of the crater.

Photogrammetric surveys of the dome from the east were undertaken by MVO, using sites at Perches and Galway's Mountain (on the crater rim to the west southwest of Perches) on 23 March (Fig.14) and 26 April. These yielded dome volumes of 56 and 78 Mm^3 respectively (± 20%) and an average extrusion rate over that period of 7.5 m^3s^{-1} (6.4 m^3s^{-1} dense rock equivalent). These estimates include the talus component of the dome, which is more visible from these two sites than from JBH and Runway (Fig. 14), but not the pyroclastic flow deposits. Set in the wider context of the third episode of dome growth from August 2005 to March 2007 [*Loughlin et al*., 2006], the AVTIS observation period corresponds to the start of a period of increased magma flux. In the context of the first episode discussed in terms of rockfall seismicity by *Calder et al*. [2005] this period would be classed as one of high extrusion rate.

6.2 AVTIS measurements of the growth of the dome and talus

From the AVTIS measurements and the surface differences generated (Figs. 7,8) it is clear that: (i) the summit of the dome rose, (ii) some large masses of the dome lava collapsed, and (iii) the lower talus slopes generally rose by deposition. While there is evidence of talus deposition around most of the observed slopes from the north to the southeast, the southeastern sector received most of the talus in the second half of the interval. This agrees with the photographic observation above.

From the daily-average intensity images of the dome (four examples shown in Fig.10) and the range data, measurements of the areal increments of lava added to the summit (Fig.9) along the AVTIS LOS have been made for each occupation (Table 4). Note that we cannot use the range-derived surface differencing method here because, generally, the summit data do not overlap (Fig.9). Lack of detailed observations of the western side of the dome summit prevents an accurate measurement of the whole summit area. Nevertheless, we can estimate the incremental volumes of lava added and lost to the summit by assuming each observed profile is representative of a 200 m diameter cap of lava. These estimates are shown in Table 4 and their cumulative volumes in Fig.15. Uncertainties of about 30-50% are considered likely. Given that we think that most of the lava extrusion was directed towards the eastern side of the summit, this assumed radial symmetry means that the volumes may be over-estimated. The volume of lava remaining at the summit increased generally in a similar way in both datasets, though at a faster rate later in the measurement period. The exception is the interval between 2 and 3 April for the JBH record, when a net reduction in height was recorded. This implies a significant collapse volume for this interval. Table 4 shows that both datasets record a notable

increase in lava added between 5 and 6 April. Averaging the two datasets gives a total addition to the summit of about 1.7 Mm^3 of lava over the eleven-day interval from 30 March to 9 April.

The volume of the new talus "hidden" from AVTIS during this period (Fig. 9) can be estimated for the area thought to be actively receiving mass wasting. This has an area of about 0.4 km^2 (Fig.6). AVTIS surface differencing accounted for the volumetric change over areas of about 0.07 km^2 from both Runway and JBH sites (Table 4), about 17% of the total, active area. We now assume that the daily volumetric changes measured by AVTIS, averaged when there is near-contemporaneous Runway and JBH data (Table 4), can be extrapolated to the whole of the area of active talus in proportion to the areas concerned (Table 5). The total talus volume thus produced (7.2 Mm^3) gives an average production rate of 7.6 m^3s^{-1} over the eleven days of the study. Such values may be underestimated because much of the extrapolated area is at lower elevation and thus there are relatively fewer "source" areas of mass loss, and it also has a generally lower gradient than the AVTIS-measured areas and so deposition should be more likely. On the other hand, use of the observed areas may have overestimated the volume deposited in the south. This compares with the 11 m^3s^{-1} estimate derived from the much simpler geometrical model of talus growth in section 5.2.

6.3 Photographic observations of rockfall and pyroclastic flow runout

Several sources of photographic information were used to estimate the runout distances of rockfalls and pyroclastic flows measured from their source near the summit of the dome. These included hand-held, and tripod-mounted, still and video cameras at the AVTIS measurement sites and the MVO automated camera at the Windy Hill site (Fig. 1), which captures images every minute and was available from 1 to10 April. The distal extent of these rockfalls and flows generally could not be seen directly in these images, but their locations were inferred from the image positions of the turbulent buoyant ash plumes that the flows generated relative to the background topography. These estimates were made to the nearest 100 metres. The flow runout values generated in this way are likely to be under-estimates in some cases because the wind was almost always from the east during this period, the same direction as the majority of flows, and tended to blow the ash plumes westwards as they rose. The one-minute interval images were more susceptible to this effect, the video data less so. The longest runout pyroclastic flow that was observed reached 1800 m from the dome summit at about 14:30 UTC on 2 April. Rockfalls that were observed to remain within the limit of the talus (~ 500 m runout) were assigned a runout of 300 m. Almost all the observed events could be correlated with the equivalent seismic record, 70 events out of a total of 1053 RF and LPRF events. The disparity between these two figures is largely accounted for by lack of visual observations during the night and during periods when cloud covered the volcano. Pyroclastic flows could sometimes be observed emerging below the cloud base, whereas rockfall events at that time would be unobserved visually.

6.4 Estimates of pyroclastic flow volumes beyond the talus

The volumes of the pyroclastic flow deposits over this interval have not been surveyed directly. Instead, we have used the rockfall seismicity of the larger recorded events as a

proxy measurement. From the correlation between the observed runout estimates and the seismic data for the same events we estimate the runouts of all the events. Assuming a runout distance to volume relationship, we can then estimate the total volume of material deposited outside the dome/talus during the observation period.

Generally, the duration of the seismic events increased as the runout increased (Fig. 16a), as did the seismic energy content (Fig.16b). The duration of an RF/LPRF event is assumed to be equivalent to the mass (volume) involved. Video-based estimates of the rate of advance of pyroclastic flows beyond the talus indicate values in the range 15-5 m/s, which agrees well with the 8 m/s linear relationship of Fig.16a, suggesting that longer duration involves increasing the flow distance (seismic excitation path). Extended (non-instantaneous) collapse events will tend to cloud this relationship. The energy of each RF/LPRF event depends on the efficiency of conversion of kinetic to seismic energy. Individual blocks impacting the talus during rockfall should be a simple transfer relationship, but disaggregation of blocks and fluidisation in a pyroclastic flow reduces the energy transfer into the ground. *Herd et al*. [2005] argued that the integrated seismic energy is proportional to the volumetric flux of the flow, but we prefer to use the duration-runout relationship here. Field observations of flow deposits at Soufrière Hills that extend just beyond the talus typically show variations between thin (0.2 m thick), sheet-like (100 m wide) deposits to channelised/lobate deposits (10-30m wide; 0.5-2 m thick) [*Cole et al*., 2002, Fig.9a] giving cross sectional areas in the range 5 – 50 m^2. *Calder et al.* [2002] suggested volumes up to 1000 m^3 as typical for rockfalls with runouts up to 500 m. Using the above range of cross sectional areas, the volumes of deposits at 1 km runout would be 3,500-26,000 m^3 which brackets the value for 1 km runout deposits of 10,000 m^3 suggested by *Calder et al.* [2002]. For flows up to 2 km runout, volumes of up to about 100,000 m^3 have been estimated [*Cole et al.,* 2002]. We use these three volume-runout pairs: (10^3 m^3 at 500 m, 10^4 m^3 at 1000 m and 10^5 m^3 at 2000 m) to define the volume-runout relationship and to calculate the volumes of all the RF/LPRF events with runouts greater than 500 m based on duration. We estimate the uncertainties on these volume at about 60%. For the period of 9-10 April when durations could not be calculated because all instruments except MBLY were inoperative, we have replicated the previous set of events from 8 April. We justify this on the grounds of the similarity of the energy characteristics measured at MBLY over the two periods. The total volume of pyroclastic flows for the 30 March to 9 April period estimated in this way is 1.8 M m^3.

Combining the estimate of pyroclastic flow deposit volume (1.8 Mm^3) with the estimates for the talus volume (7.2 Mm^3) and summit lava (1.7 Mm^3) gives a total of 10.7 Mm^3 for the eleven-day period (Table 5). Figure 13 shows the cumulative daily totals for the talus, talus plus summit lava and all three sources together. Up to 5 April the output is nearly linear. After that the contribution from the summit lava increases and the overall output rate increases. The equivalent daily seismic energy release shows a different pattern (Fig.17), with a gradual reduction from 31 March to 6 April, followed by a much a higher rate. Both datasets show the same contrast between modest rates in the first part of the record and the much more vigorous second period. The main difference is that the volumetric estimates show a rise on 5 April, whilst the inflection in the cumulative

rockfall seismic energy occurs on 7 April. Our interpretation of this is that the lava supply rate did increase on 5 April but had the effect of building up a new mass of lava at the summit. Rockfalls that did occur were smaller than usual and fewer were recorded as events from the seismometer network. For 5 and 6 April the rockfall seismicity was not a good proxy for the high lava extrusion rate, but from 7 April onwards the size and number of rockfall events increased greatly as the high rate of extrusion was maintained. It is possible that this lag in behaviour was due to the re-orientation of the extrusive vent .

7. Discussion

From our measurements and estimates, the proportion of extruding lava that remained within the lava core of the dome during this interval was about 16%. This is a low proportion compared to the earliest, endogenous, stages of lava dome growth, at Soufrière Hills and other volcanoes, when the proportion of non-talus growth can approach 100%. The occurrence of just one or two larger collapses, of which there were none in this interval, would change this figure significantly, and a longer sampling interval would yield a more accurate estimate of the long-term pattern. A similar argument can be made for the pyroclastic flow deposit volumes, which account for about 17% of the extruded volume during our observations. However, this third episode of dome growth (since August 2005) has been less prone to frequent collapse events than during the earlier two episodes of extrusion. For example, during the first half of 1997, when the lava extrusion rate was less than 5 m^3s^{-1} the dome: pyroclastic flow volume ratio was about 60:40, but this became about 40:60 when the extrusion rate rose to about 10 m^3s^{-1} during the second half of 1997 [*Sparks et al*., 1998]. This contrasts strongly with the 83:17 ratio measured here during similar extrusion rates. The average extrusion rate over the eleven days was 11.2 m^3s^{-1}. The bulk density of the talus, and lava components of the dome during March-April 2006 were not measured, but following *Sparks et al*. [1998], a factor of 0.86 can be used to convert from vesicular lava to dense rock equivalent. This gives a dense rock equivalent total production rate of 9.7 m^3s^{-1}, and for the non-pyroclastic flow components a rate of 8.1 m^3s^{-1}, compared to the equivalent 6.4 m^3s^{-1} measured by photogrammetry for the 23 March - 26 April period.

The high proportion of extruded lava that is converted to talus revealed by this study has implications for hazard analysis. Lava that remains in the core of the dome can retain much more heat and gas content and sustain greater overpressures than the surrounding apron of lava talus. It is the sudden depressurization of this lava that can lead to the generation of large, mobile pyroclastic flows and even lateral blasts (e.g. Woods et al., 2002). Thus if the high degree of conversion of lava to talus measured in this study is representative in the longer term, then the total volume of highly pressurized core lava will be less. This may reduce the propensity for hazardous pyroclastic flows.

The daily-averaged AVTIS measurements show that the actual dome growth departs somewhat from the self-similar frustum geometrical model. The uppermost slopes of the dome, that expose the core lava and have the highest gradients (> 40º), tend not to accumulate new mass and occasionally shed large volumes. This is exemplified by the

differences in profile between Figs. 9 and 11. Our data were not sufficient to determine whether any differential volume accumulation on different slopes was occurring. During the measurement period there were several departures from the steady state, incremental view of the mass wasting process at the dome as a series of rockfalls (individually unmeasurable by AVTIS), continually transporting mass from the dome summit to the talus. A major loss of mass from the upper eastern part of the dome appears to have occurred on 31 March, during one of the large rockfall events. Downslope from this, mass was accumulating as early as 2 April and particularly after 5 April, and both the Runway and JBH records show deposition increasing to the southeast. A 40 m increase in the elevation of the dome summit appears to occur primarily between 5 and 6 April at the time of a minimum in the number and energy of RF/LPRF events. This could represent a minor change in the vent extrusion direction as new mass accumulates at the summit. However, despite the reduction in rockfall numbers, the rate of addition to the AVTIS-measurable talus area does not slacken. This may be because these lower energy rockfalls deposited their mass more proximally than at other times.

Throughout, we have assumed that the dome growth process measured by AVTIS was entirely exogenous. That is, all the rising magma reached the surface near the summit of the dome and none was added internally to swell the dome. There is no reason to doubt this, but AVTIS range change alone is not enough to distinguish between surface deposition and swelling.

There is no doubt that AVTIS could yield much more valuable information on the dome growth process with improved temporal and spatial resolution. Rockfalls with typical volumes in the range 10^3 – 10^4 m^3 occurred about every 15 minutes during our experiment. From a closer viewpoint, with improved signal-to-noise strength and faster scan speed it should be feasible to detect the sources and deposits of individual rockfalls. This would enable us, by combining this information with rockfall seismology, to explore the dynamics of the process more fully. Also a continuous audit of the dome core versus talus volumes would help to evaluate the hazard posed by future large pyroclastic flows involving core lava.

Acknowledgements

Dr Vicky Hards is thanked for help with camera data. We are grateful to NERC for grant NE/E001734/1 to undertake this work and for their earlier support of the development of AVTIS. GR, SDA and SCL publish with the permission of the Director, British Geological Survey (NERC).

References

Calder, E.S., R. Luckett, R.S.J. Sparks, and B. Voight (2002), Mechanisms of lava dome instability and generation of rockfalls and pyroclastic flows at Soufrière Hills Volcano, Montserrat. In, Druitt, T.H. and B.P. Kokelaar (eds.) *The eruption of*

Soufrière Hills Volcano, Montserrat, from 1995 to 1999. Geological Society, London, Memoirs, 21, 173-190.

Calder, E.S., J.A.Cortes, J.L. Palma, and R. Luckett (2005), Probabilistic analysis of rockfall frequencies during an andesite lava dome eruption: the Soufriere Hills Volcano, Montserrat. *Geophys. Res. Lett., 32*, L16309, doi:10.1029/2005GL023594.

Davies, T.R., M.J. McSavenny, and K.A. Hodgson (1999), A fragmentation-spreading model for long-runout rock avalanches. *Can. J. Geotech*., *36*, 1096-1110.

Hort, M., M. Voge, R. Seyfried, and A. Ratdomopurbo (2006), In situ observation of dome instabilities at Merapi volcano, Indonesia: a new tool for volcanic hazard mitigation. *J. Volcanol. Geotherm. Res*., *153*, 301-312.

Jones, L.D. (2006), Monitoring landslides in hazardous terrain using terrestrial LiDAR: an example from Montserrat. *Quat. J.Eng. Geol. Hydrogeol*., *39*, 371-373.

Luckett, R., B. Baptie, and J. Neuberg (2002), The relationship between degassing and rockfall signals at Soufrière Hills Volcano, Montserrat. In, Druitt, T.H. and B.P. Kokelaar, (eds.) *The eruption of Soufrière Hills Volcano, Montserrat, from 1995 to 1999*. Geological Society, London, Memoirs, 21, 595-602.

Loughlin, S., B. Baptie, T. Christopher, G. Ryan, R. Luckett, V. Hards, L. Jones, N. Fournier, V. Bass, T. Syers, L. Ruzié, M. Higgins, P. Williams, and D. Williams (2006) Report to the Scientific Advisory Committee, Montserrat, August 2006. *MVO Open File Report* 06/07, 39pp.

Macfarlane, D.G., G. Wadge, D.A. Robertson, M.R. James, and H. Pinkerton (2006), Use of a portable topographic mapping millimetre wave radar at an active lava flow. *Geophys. Res. Lett*., *33*, L03301, doi:10.1029/2005GL025005.

Macfarlane, D.G. and D.A. Robertson (2004), AVTIS – a dual-mode imaging millimetre wave radar/radiometer for volcanological surveying. *Proc. IGARSS'04* Anchorage, Alaska, September 2004, Vol. V, 3299-3302.

Macfarlane, D.G. and D.A. Roberston (2006), A 94GHz real aperture 3D imaging radar, *3rd European Radar Conference,* Manchester, UK, September 2006, pp154 -157, doi: 10.1109/EURAD.2006.280297

Okura, Y., H. Kitahara, T. Sammori, and A. Kawanami (2000), The effects of rockfall volumes on runout distance. *Eng. Geol*., *58*, 109-124.

Sato, H., T. Fujii, and S. Nakada (1992), Crumbling dacite dome lava and generation of pyroclastic flows at Unzen Volcano. *Nature*, *360*, 664-666.

Sparks, R.S.J. and 19 others (1998), Magma production and growth of the lava dome of the Soufriere Hills Volcano, Montserrat, West Indies: November 1995 to December 1997. *Geophys. Res. Lett*., *25*, 3421-3424.

Vaughan, R.G., S.J. Hook, M.S. Ramsey, V.J. Realmuto, and D.J. Schneider (2005), Monitoring eruptive activity at Mount St. Helens with TIR image data. *Geophys. Res. Lett*., *32,* L19305, doi:10.1029/2005GL024112.

Wadge, G., (2007), Assessing the pyroclastic flow hazards at Soufriere Hills Volcano, Montserrat. In: *Advances in Volcanology: the legacy of G.P.L. Walker* (in review).

Wadge, G., D.G. Macfarlane, D.A. Robertson, A.J. Hale, H. Pinkerton, R.V. Burrell, G.E. Norton, and M.R. James, M.R. (2005), AVTIS: a novel millimetre-wave ground based instrument for volcano remote sensing. *J. Volcanol. Geotherm. Res*. *146*, 307-318.

Wadge, G., D.G. Macfarlane, M.R. James, H.M. Odbert, L.J. Applegarth. H. Pinkerton,

D.A. Robertson, S.C. Loughlin, M. Strutt, G. Ryan, P.N. Dunkley (2006), Imaging a growing lava dome with a portable radar. *EOS*, AGU 87/23, 226-228.

Watts, R.B., R.A. Herd, R.S.J. Sparks, and S.R. Young, S.R. (2002), Growth patterns and emplacement of the andesitic lava dome at Soufriere Hills, Montserrat. In, Druitt, T.H. and B.P. Kokelaar (eds.) *The eruption of Soufrière Hills Volcano, Montserrat, from 1995 to 1999*. Geological Society, London, Memoirs, 21, 115-152.

Woods, A.W., R.S.J. Sparks, L.J. Ritchie, J. Batey, C. Gladstone, and M.I. Bursik, (2002). The explosive decompression of a pressurized volcanic dome: the 26 December 1997 collapse and explosion of Soufrière Hills Volcano, Montserrat. In, Druitt, T.H. and B.P. Kokelaar (eds.) *The eruption of Soufrière Hills Volcano, Montserrat, from 1995 to 1999*. Geological Society, London, Memoirs, 21, 457-465.

Figure Captions

Fig. 1 Map of the northeastern slopes of Soufrière Hills Volcano, Montserrat as of April 2006 showing the locations (crosses) of AVTIS sites for measurements to the lava dome, the locations of seismometers MBLY and MBGH (triangle), and the automatic camera at Windy Hill (diamond). Contour interval is 50 m with bold contours at 250 m intervals. Local topographic grid interval in km.

Fig. 2 Schematic cross section through the Soufrière Hills Volcano lava dome showing the lava shear lobe fragmenting to talus through rockfall. Right-hand scale is in metres above sea level.

Fig. 3 The relationship between signal-to-noise ratio (SNR) and AVTIS range accuracy as determined from a Monte Carlo analysis. SNR is taken as the ratio of signal amplitude (filtered in range and over multiple individual scans: 14 for JBH and 10 for St. George's Hill)) to the 95th percentile of the noise distribution. Synthetic values of SNR were obtained by applying scaling factors to AVTIS spectra measured at JBH (squar,e labelled 0) in increments of ± 1 dBm and St. George's Hill (circle, labelled 0) in increments of ± 3 dBm. Range accuracy is measured as the standard deviation (in metres) of range values acquired for 1000 simulated power spectra, using the Monte Carlo method. The inset panel shows a typical power spectrum measured against range from St. George's Hill in which the dome is seen as a peak in returned power at ~3 km. Solid black lines show the filtered spectrum and two example synthetic spectra, attenuated to -6dBm and +6dBm (labelled 0, –6 and +6 respectively).

Fig. 4 Schematic of the field deployment of AVTIS. The distant lava dome is imaged as a raster built up using a pan-and-tilt gimbal. C1 and C2 are tripod-mounted corner cube reflectors at distances of several hundred metres used to provide absolute pointing knowledge for AVTIS. The top left panel shows a schematic cross section through the footprint of the radar beam on the dome surface during a single LOS measurement. R1 and R2 are the near and far ranges of the footprint and Rmax is the dominant reflector whose range will be taken as the range value for that LOS measurement.

Fig. 5 Standard deviation of fourteen values of range measured for every LOS from Jack Boy Hill to the lava dome on 2 April, plotted against the corresponding angles of incidence onto the surface (all circles and fitted dashed curve). The filled circles and solid curve (four-term polynomial) are the subset of data that are at least 0.3º away from margins of the dome.

Fig. 6 Map of the dome and crater. The fine dashed and thick solid lines denote the approximate areas on the dome covered by AVTIS from the Jack Boy Hill and Runway sites respectively.The area of the dome covered by lava is shown in white, the area covered by talus in pale grey and the area of pyroclastic flow deposits in darker grey. The thick dashed line denotes the southwestern boundary of active mass wasting. The position of the vent for the dome is shown by the circle, the solid line leading from it is the line of

the profile in Fig. 10. The cross marks the Perches viewpoint and contours are shown every 50 m above sea level.

Fig. 7 Changes in the surface elevation of the lava dome measured from Runway between the dates shown (e.g. 30 – 31 is the difference between 30 and 31 March 2006). The elevation scale is in metres, contoured at 5 metre intervals. The dashed line in the 30 - 31 panel represents the approximate position of the lava/talus boundary.

Fig. 8 Changes in the surface elevation of the lava dome measured from Jack Boy Hill between the dates shown (e.g. 2-3 is the difference between 2 and 3 April 2006). The elevation scale is in metres, contoured at 5 metre intervals. The dashed line in the 2-3 panel represents the approximate position of the lava/talus boundary.

Fig. 9 Comparison of two profiles through the surfaces measured by AVTIS from Runway on 30 March and 7 April. The dashed portions of the lines are inferred. The orientation of the profile is shown by the solid line in Fig.6.

Fig.10 AVTIS intensity images of the lava dome. a and b are occupation (2 and 11) averages of intensity collected on 30 March and 6 April from the Runway site, c and d are occupation averages (5 and 17) collected on 2 April and 9 April from the JBH site. The colour scales represent about a 7 dB range for the Runway images and about 5 dB for the JBH images. The pixels on the dome represent areas of about 10 x 10 m.

Fig. 11 Geometrical model of the dome. A right conical frustum (dome and talus) sits on a similar base. The vent for lava extrusion forms the axis of symmetry of the 3D construct by rotation. The reduction in thickness with radial distance of a rockfall depositing equal mass with constant radial increment onto the talus is shown in the plot.

Fig. 12 Number of RF and LPRF events recorded on the MVO seismic network each day.

Fig. 13 Times series showing the magnitude of energy release by individual RF and LPRF seismic events (black dots) between 30 March and 10 April 2006 (as measured from station MBGH at St. George's Hill). The black bars are the durations of the AVTIS range measurements. Times are in UTC. The off-scale event on 10 April denoted by the arrow had an energy of 9.1×10^{-6} J/kg. The data between 08:00 on 9 April and 13:00 on 10 April are data from station MBLY calibrated to MBGH energy levels.

Fig. 14 Photographs of the dome from the Perches site (Fig.1) on 23 March 2006 (top), 10 April 2006 (middle), and a sketch of the margins of the dome and talus on the two dates to emphasize the changes (bottom). X shows the location of a large mass of dome lava that disappeared after 23 March.

Fig. 15 Cumulative volume of lava at the summit of the dome over the period 30 March to 9 April 2006, estimated from the AVTIS intensity and range measurements made from the Runway (solid line) and Jack Boy Hill (dashed line) sites.

Fig. 16 Observed pyroclastic flow runout distances plotted against (a) the signal duration recorded by the seismometer network , and (b) the energy release measured at station MBGH (arrowed event has an energy of 17.10^{-7} J/kg). The line in (a) represents a rate of 8 m/s.

Fig. 17 Cumulative daily volumes of talus (thin solid line), talus and summit lava (medium solid line). and talus, summit lava and pyroclastic flow deposits (thick solid line). Values from Table 5. Also plotted is the cumulative seismic energy from the MBGH station.

Table 1. AVTIS technical characteristics

Parameter	**Value**
Frequency	94GHz
Radar Range Resolution	0.85m
Radiometric Thermal Sensitivity	<5K
Antenna Size	300mm
Two-way Radar Beamwidth	0.5º
Radiometric Beamwidth	0.7º
Radar Transverse Resolution (per km)	8.7m
Radar Signal-to-Noise at Long Range	6dB (@7km)
Data Sampling Rate	500kHz
Maximum Pixel Integration Time	32ms
Image Acquisition Time (10^ox5^o,0.1^o inc.)	20min
Power Consumption	115W
Continuous Operational Duration	8 hours

Table 2. Occupations numbered in chronological order with number of images per occupation in brackets and time span (UTC) of acquisition periods from different localities

Date	**Runway**	**JBH**	**Spanish Point**	**White's Yard**	**Perches**	**SGH**
Elevation (m asl)	6	196	31	191	786	352
Azimuth (deg.)	201	186	210	219	286	103
30 March	1 (5) 15:53-20:25					
31 March	2 (4) 15:25-18:41	3 (0)				
1 April						4 (14) 13:22-17:31
2 April		5 (14) 15:10-01:44				
3 April	6 (1) 19:20-19:51	7 (8) 22:54-02:14				
4 April			8 (4) 15:30-19:53			
5 April	9 (4) 16:07-19:13	10 (7) 21:51-02:27				
6 April	11 (2) 15:34-19:24	12 (5) 20:34-22:43				
7 April	13 (3) 16:14-20:17	14 (15) 22:09-07:49				
8 April		15 (11) 14:39-22:06				
9 April		17 (4) 20:54-23:59				16 (5) 15:56-17:55
10 April				18 (2) 15:17-15:32	19 (1) 16:50-17:23	

Table 3. Maximum dome elevations and incremental summit lava volume estimates derived from AVTIS data collected at Runway and Jack Boy Hill sites

Date	Maximum elevation from Runway (m asl)	Maximum elevation from JBH (m asl)	Summit lava volume increment from Runway (10^3 m^3)	Summit lava volume increment from JBH (10^3 m^3)
30 March	910			
31 March	910		35	
1 April				
2 April		920		
3 April		910		-422
4 April				
5 April	920	910	246	317
6 April	950	940	1020	651
7 April	950	940	229	88
8 April		930		475
9 April		940		264

Table 4. Cumulative and daily averaged volumetric differences between the surfaces measured by AVTIS from the Jack Boy Hill and Runway sites.

Date	**Jack Boy Hill**			**Runway**		
	Occup..	Cumulative volume (10^3m^3) [area 10^3 m^2]	Daily volume (10^3m^3)	Occup..	Cumulative volume (10^3m^3) [area 10^3 m^2]	Daily volume (10^3m^3)
30 March				1	0	
31 March				2	-13 [76]	-13
1 April						148
2 April	5	0				148
3 April	7	339 [63]	339			148
4 April			76			148
5 April	10	490 [58]	75	9	727 [74]	148
6 April	12	772 [63]	282	11	1029 [72]	302
7 April	14	818 [58]	46	13	1240 [75]	211
8 April	15	875 [67]	57			
9 April	17	872 [64]	-3			

Table 5. Daily volumetric budget for lava, talus and pyroclastic flow deposits

Date	**AVTIS-area volumes (10^3m^3)**	**Active talus volumes (10^3m^3)**	**Summit lava volumes (10^3m^3)**	**Pyroclastic flow volumes (10^3m^3)**	**Daily Total (10^3m^3)**
30 March	-	-	-	39	39
31 March	-13	-68	35	58	25
1 April	148	800	49	180	1029
2 April	148	800	49	109	958
3 April	243	1409	-373	249	1285
4 April	111	673	49	111	833
5 April	111	673	183	73	929
6 April	292	1743	836	71	2650
7 April	129	770	159	162	1091
8 April	57	337	475	508	1320
9 April	-3	-19	264	281	526
Totals	1223	7206	1726	1841	10685

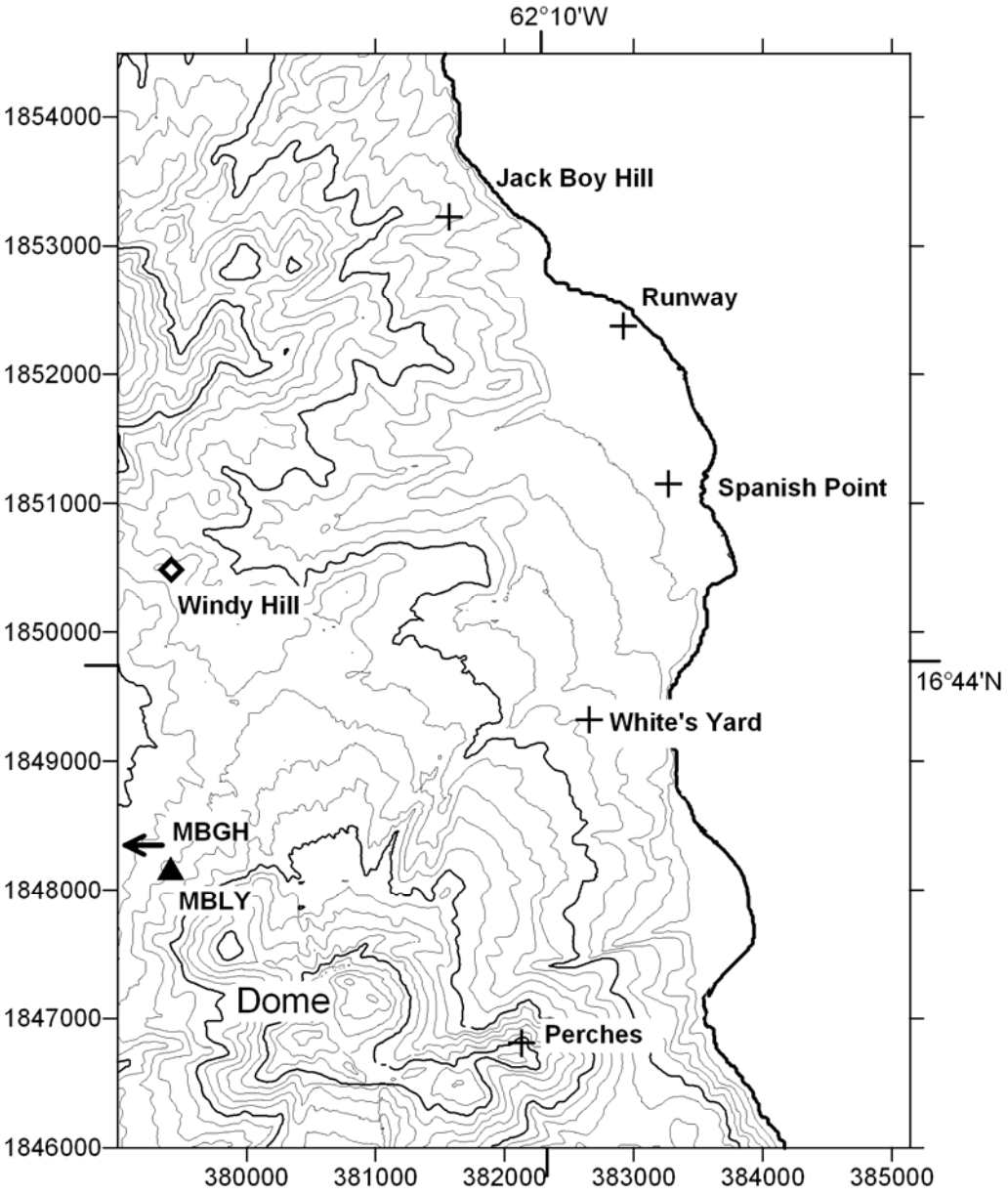

Fig.1 Map of the northeastern slopes of Soufrière Hills Volcano, Montserrat as of April 2006 showing the locations (crosses) of AVTIS sites for measurements to the lava dome, the locations of seismometers MBLY and MBGH (triangle), and the automatic camera at Windy Hill (diamond). Contour interval is 50 m with bold contours at 250 m intervals. Local topographic grid interval in km.

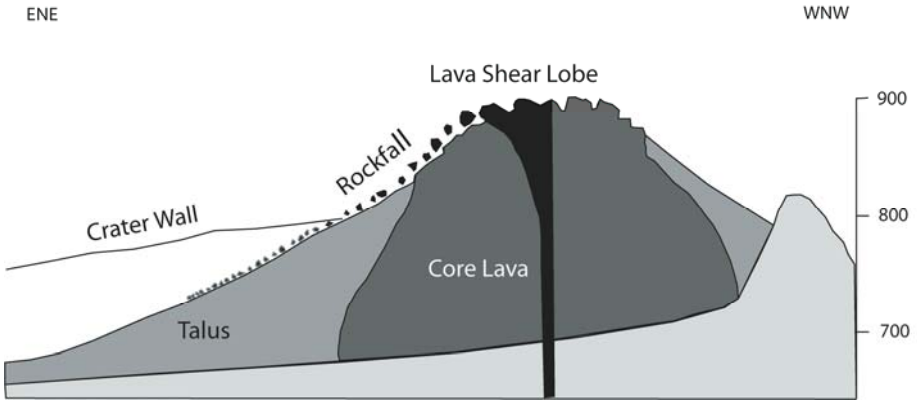

Fig. 2 Schematic cross section through the Soufrière Hills Volcano lava dome showing the lava shear lobe fragmenting to talus through rockfall. Right-hand scale is in metres above sea level.

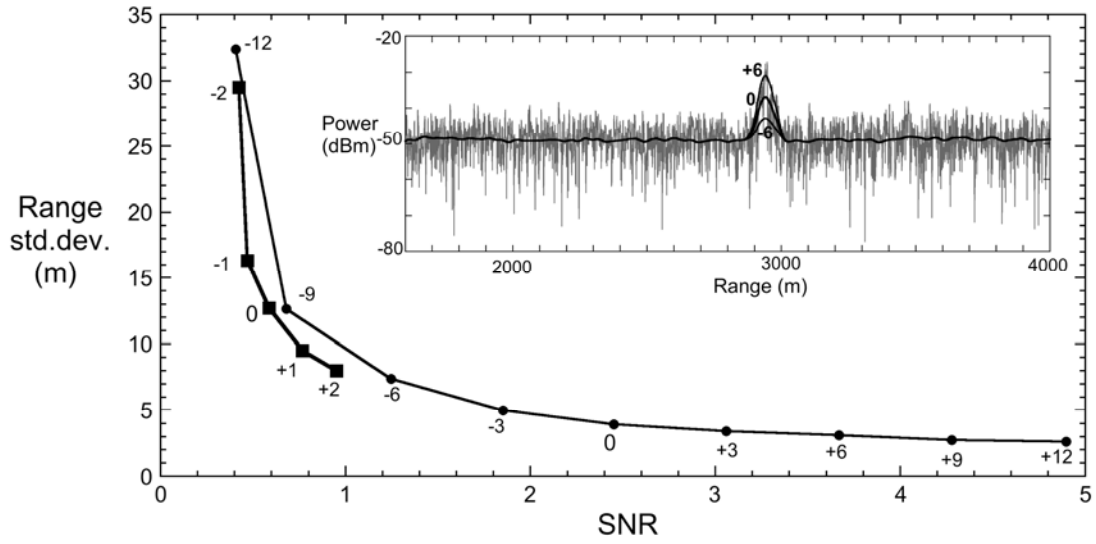

Fig. 3 The relationship between signal-to-noise ratio (SNR) and AVTIS range accuracy as determined from a Monte Carlo analysis. SNR is taken as the ratio of signal amplitude (filtered in range and over multiple individual scans: 14 for JBH and 10 for St. George's Hill)) to the 95th percentile of the noise distribution. Synthetic values of SNR were obtained by applying scaling factors to AVTIS spectra measured at JBH (squar,e labelled 0) in increments of ± 1 dBm and St. George's Hill (circle, labelled 0) in increments of ± 3 dBm. Range accuracy is measured as the standard deviation (in metres) of range values acquired for 1000 simulated power spectra, using the Monte Carlo method. The inset panel shows a typical power spectrum measured against range from St. George's Hill in which the dome is seen as a peak in returned power at ~3 km. Solid black lines show the filtered spectrum and two example synthetic spectra, attenuated to -6dBm and +6dBm (labelled 0, –6 and +6 respectively).

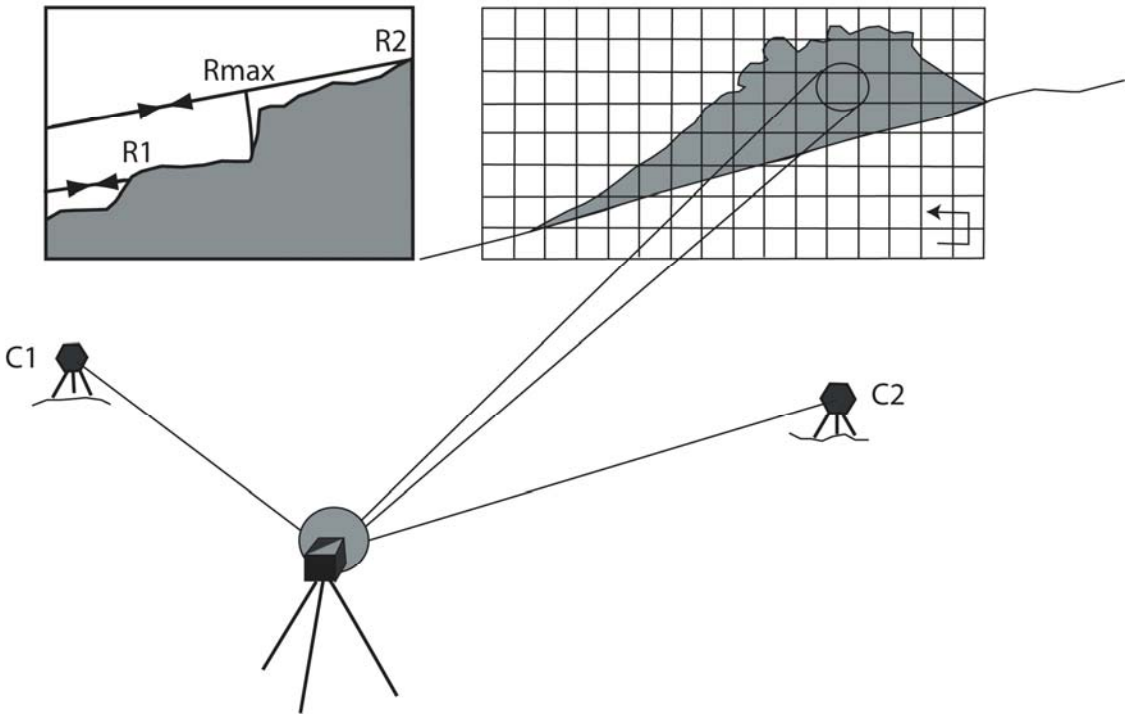

Fig. 4 Schematic of the field deployment of AVTIS. The distant lava dome is imaged as a raster built up using a pan-and-tilt gimbal. C1 and C2 are tripod-mounted corner cube reflectors at distances of several hundred metres used to provide absolute pointing knowledge for AVTIS. The top left panel shows a schematic cross section through the footprint of the radar beam on the dome surface during a single LOS measurement. R1 and R2 are the near and far ranges of the footprint and Rmax is the dominant reflector whose range will be taken as the range value for that LOS measurement.

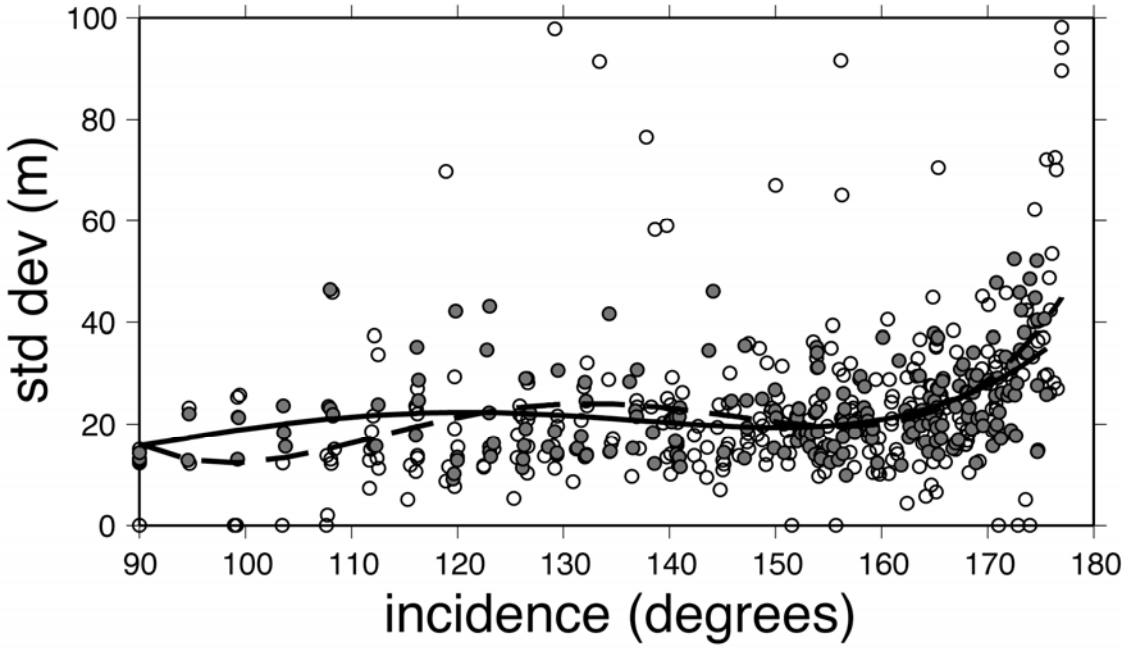

Fig. 5 Standard deviation of fourteen values of range measured for every LOS from Jack Boy Hill to the lava dome on 2 April, plotted against the corresponding angles of incidence onto the surface (all circles and fitted dashed curve). The filled circles and solid curve (four-term polynomial) are the subset of data that are at least 0.3º away from margins of the dome.

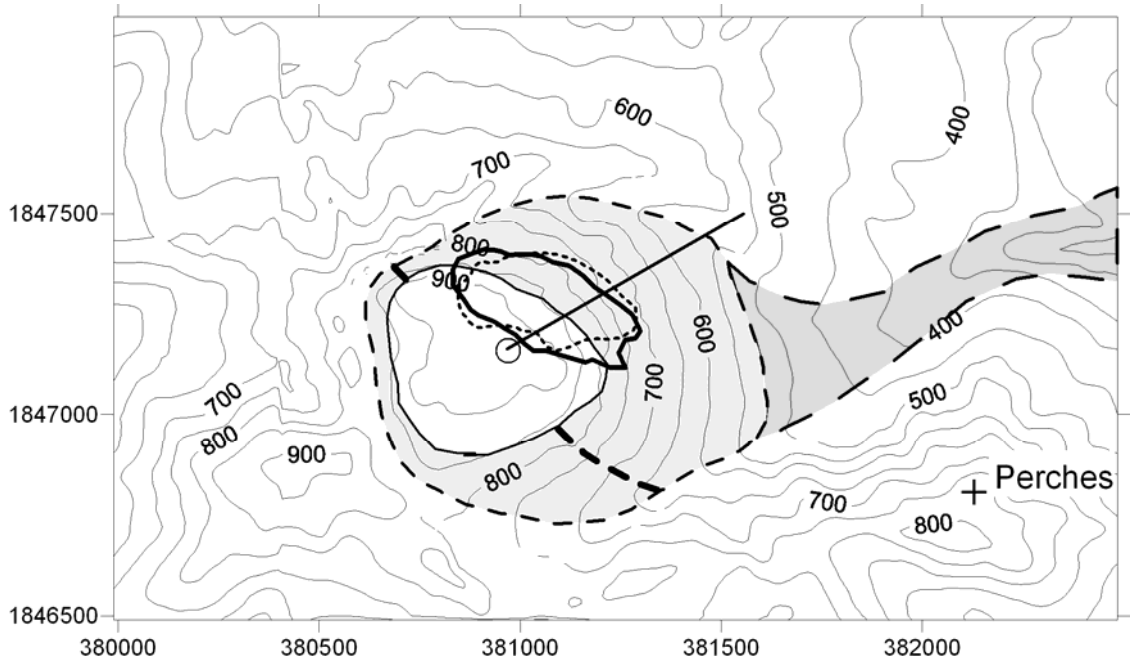

Fig. 6 Map of the dome and crater. The fine dashed and thick solid lines denote the approximate areas on the dome covered by AVTIS from the Jack Boy Hill and Runway sites respectively. The area of the dome covered by lava is shown in white, the area covered by talus in pale grey and the area of pyroclastic flow deposits in darker grey. The thick dashed line denotes the southwestern boundary of active mass wasting. The position of the vent for the dome is shown by the circle, the solid line leading from it is the line of the profile in Fig. 10. The cross marks the Perches viewpoint and contours are shown every 50 m above sea level.

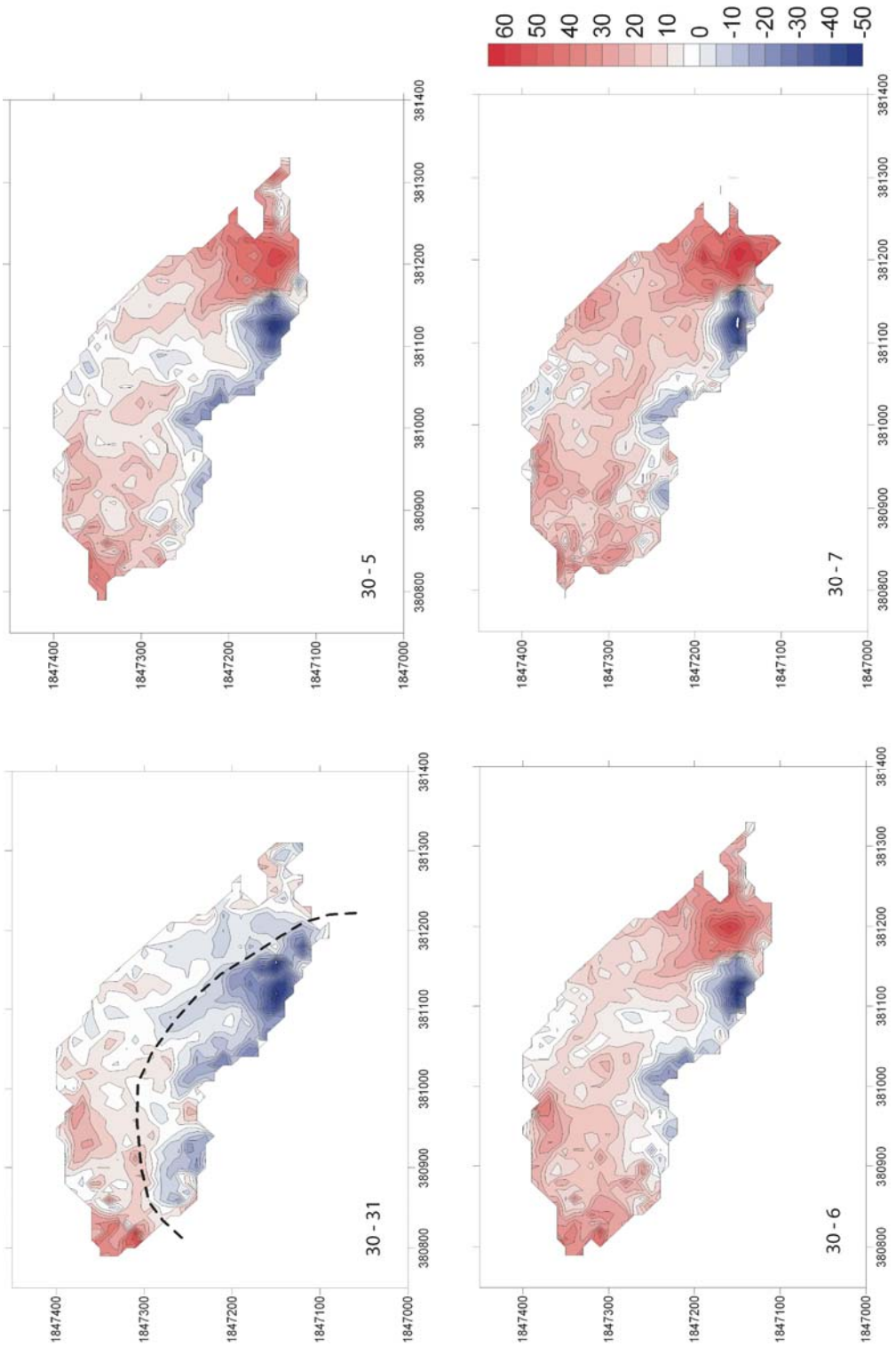

Fig. 7 Changes in the surface elevation of the lava dome measured from Runway between the dates shown (e.g. 30 – 31 is the difference between 30 and 31 March 2006). The elevation scale is in metres, contoured at 5 metre intervals. The dashed line in the 30 - 31 panel represents the approximate position of the lava/talus boundary.

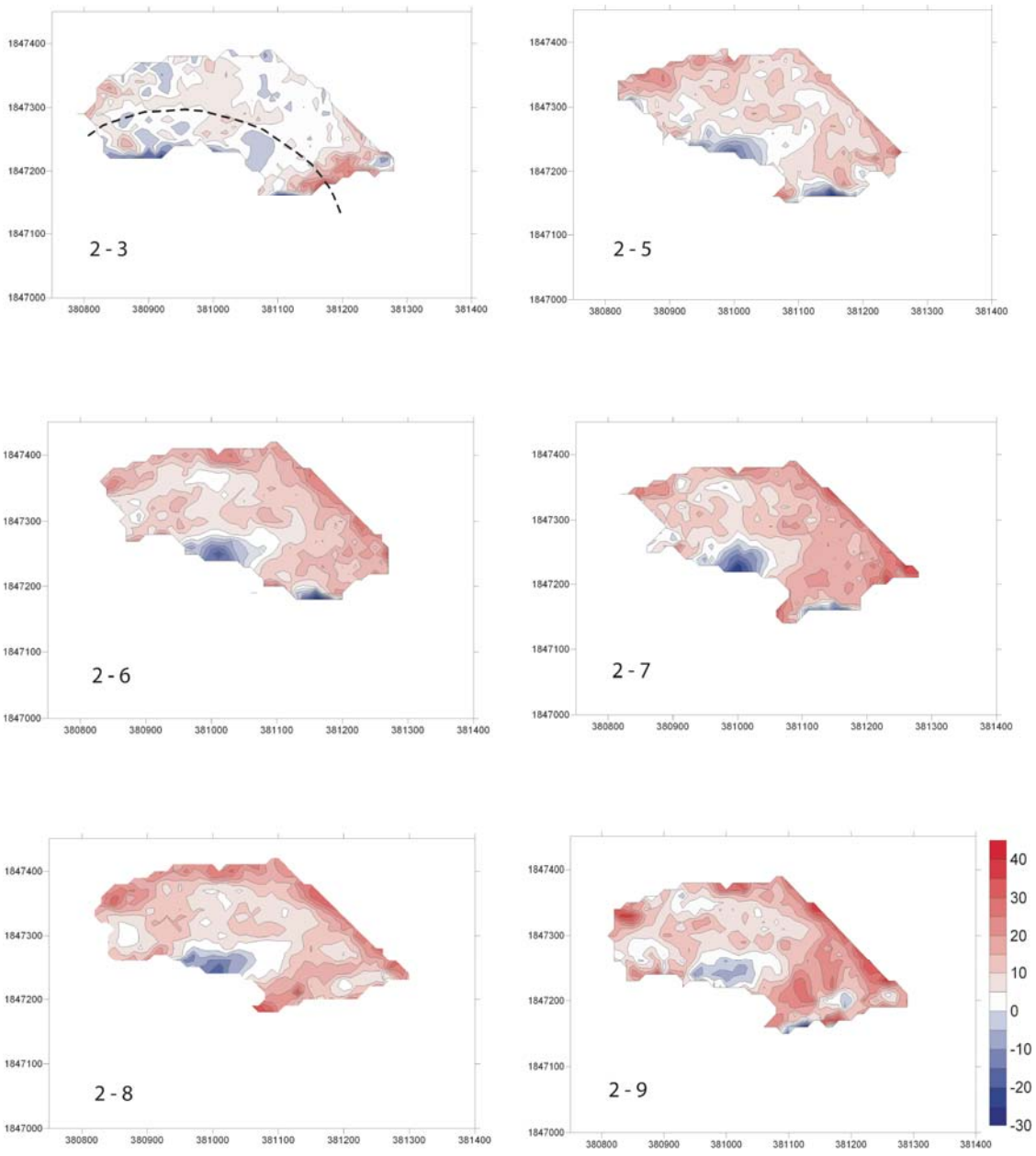

Fig. 8 Changes in the surface elevation of the lava dome measured from Jack Boy Hill between the dates shown (e.g. 2-3 is the difference between 2 and 3 April 2006). The elevation scale is in metres, contoured at 5 metre intervals. The dashed line in the 2-3 panel represents the approximate position of the lava/talus boundary.

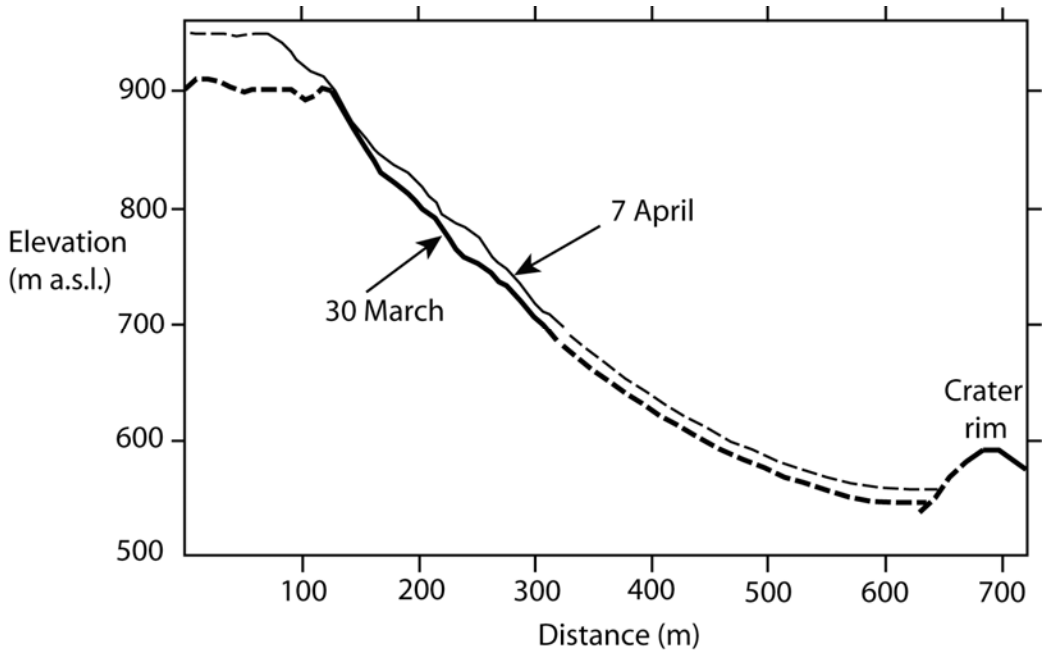

Fig.9 Comparison of two profiles through the surfaces measured by AVTIS from Runway on 30 March and 7 April. The dashed portions of the lines are inferred. The orientation of the profile is shown by the solid line in Fig.6.

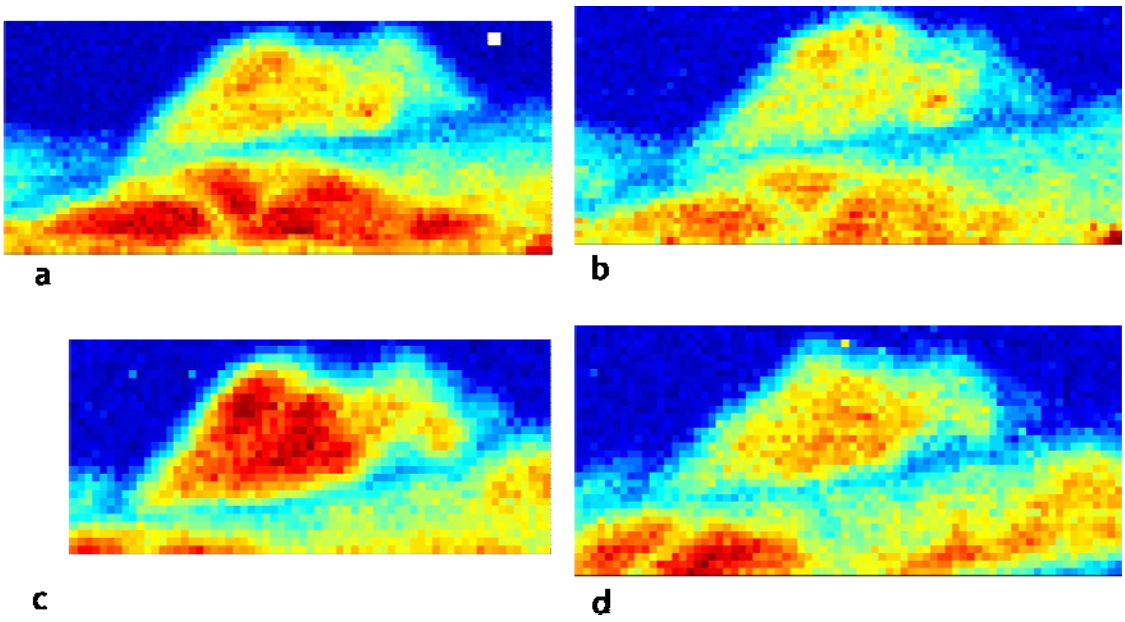

Fig.10 AVTIS intensity images of the lava dome. a and b are occupation (2 and 11) averages of intensity collected on 30 March and 6 April from the Runway site, c and d are occupation averages (5 and 17) collected on 2 April and 9 April from the JBH site. The colour scales represent about a 7 dB range for the Runway images and about 5 dB for the JBH images. The pixels on the dome represent areas of about 10 x 10 m.

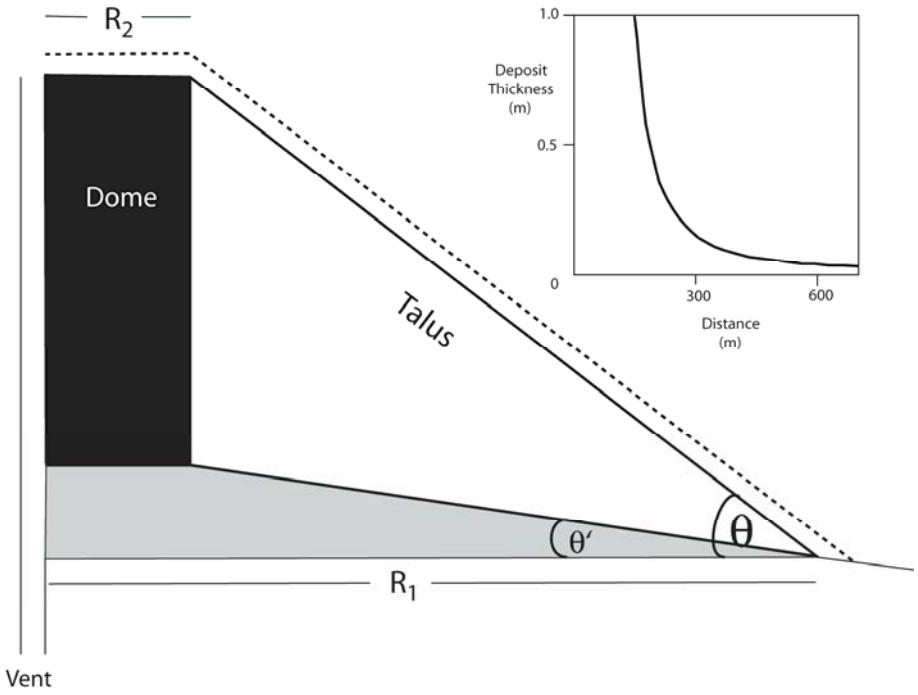

Fig.11 Geometrical model of the dome. A right conical frustum (dome and talus) sits on a similar base. The vent for lava extrusion forms the axis of symmetry of the 3D construct by rotation. The reduction in thickness with radial distance of a rockfall depositing equal mass with constant radial increment onto the talus is shown in the plot.

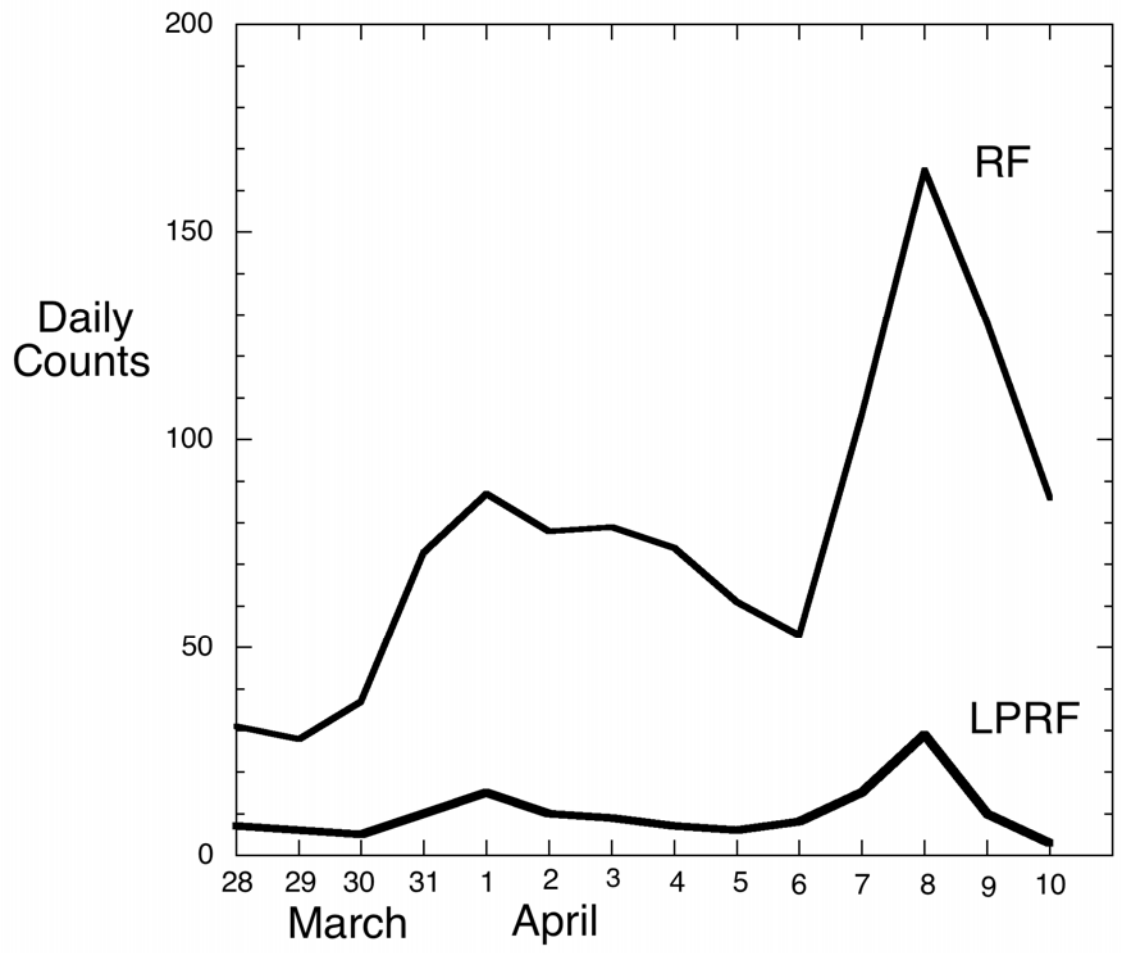

Fig. 12 Number of RF and LPRF events recorded on the MVO seismic network each day.

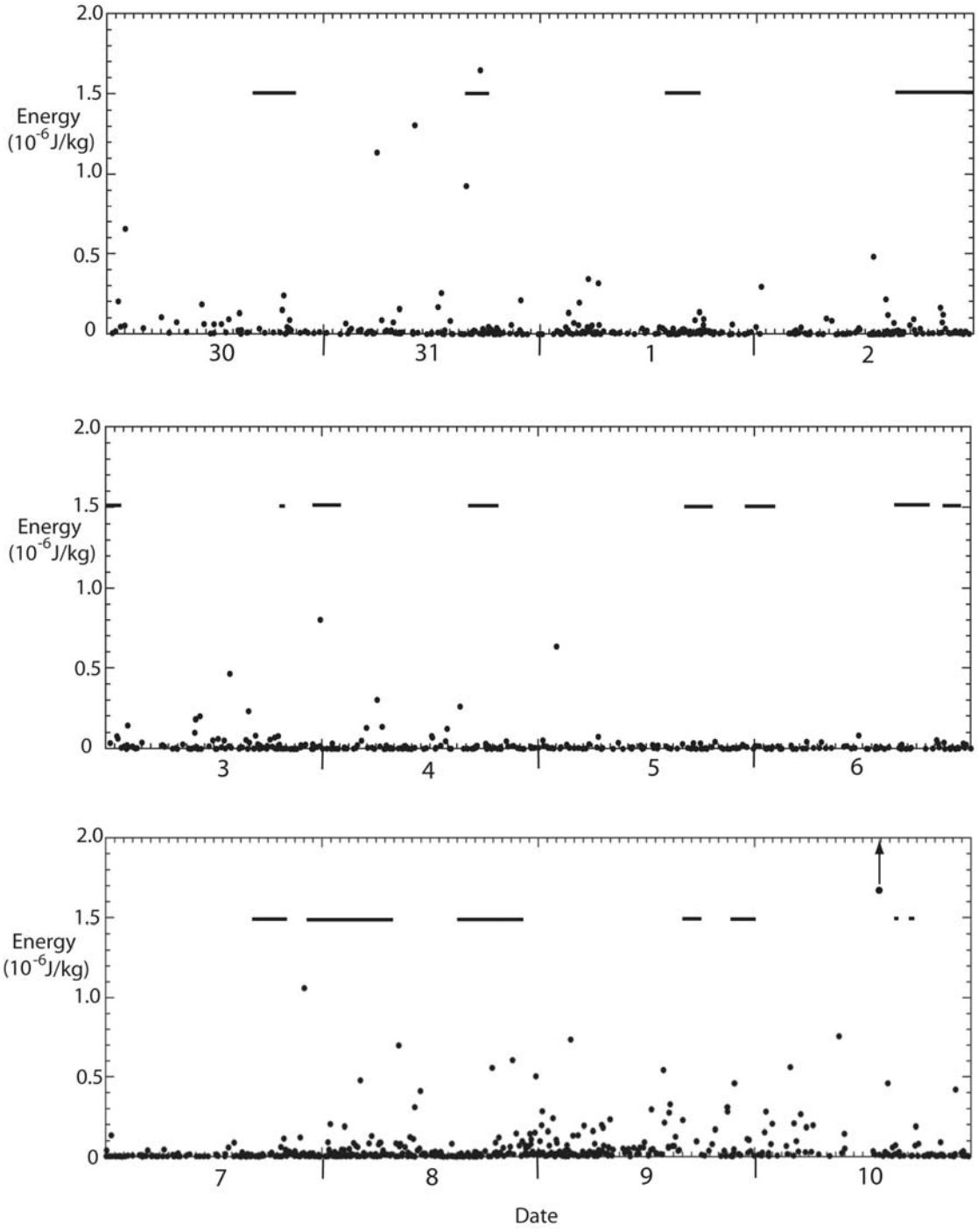

Fig. 13 Times series showing the magnitude of energy release by individual RF and LPRF seismic events (black dots) between 30 March and 10 April 2006 (as measured from station MBGH at St. George's Hill). The black bars are the durations of the AVTIS range measurements. Times are in UTC. The off-scale event on 10 April denoted by the arrow had an energy of 9.1 x 10^{-6} J/kg. The data between 08:00 on 9 April and 13:00 on 10 April are data from station MBLY calibrated to MBGH energy levels.

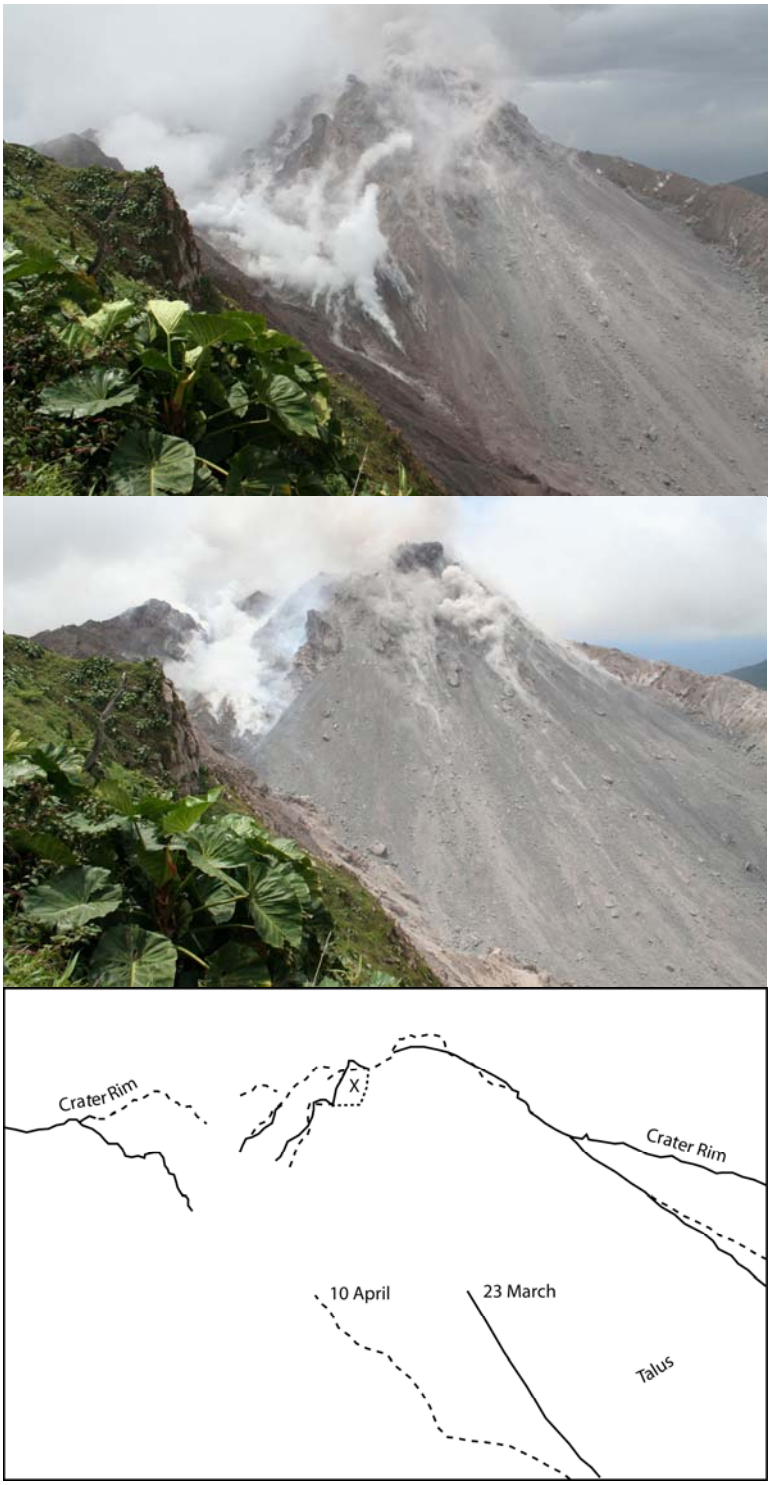

Fig. 14 Photographs of the dome from the Perches site (Fig.1) on 23 March 2006 (top), 10 April 2006 (middle), and a sketch of the margins of the dome and talus on the two dates to emphasize the changes (bottom). X shows the location of a large mass of dome lava that disappeared after 23 March.

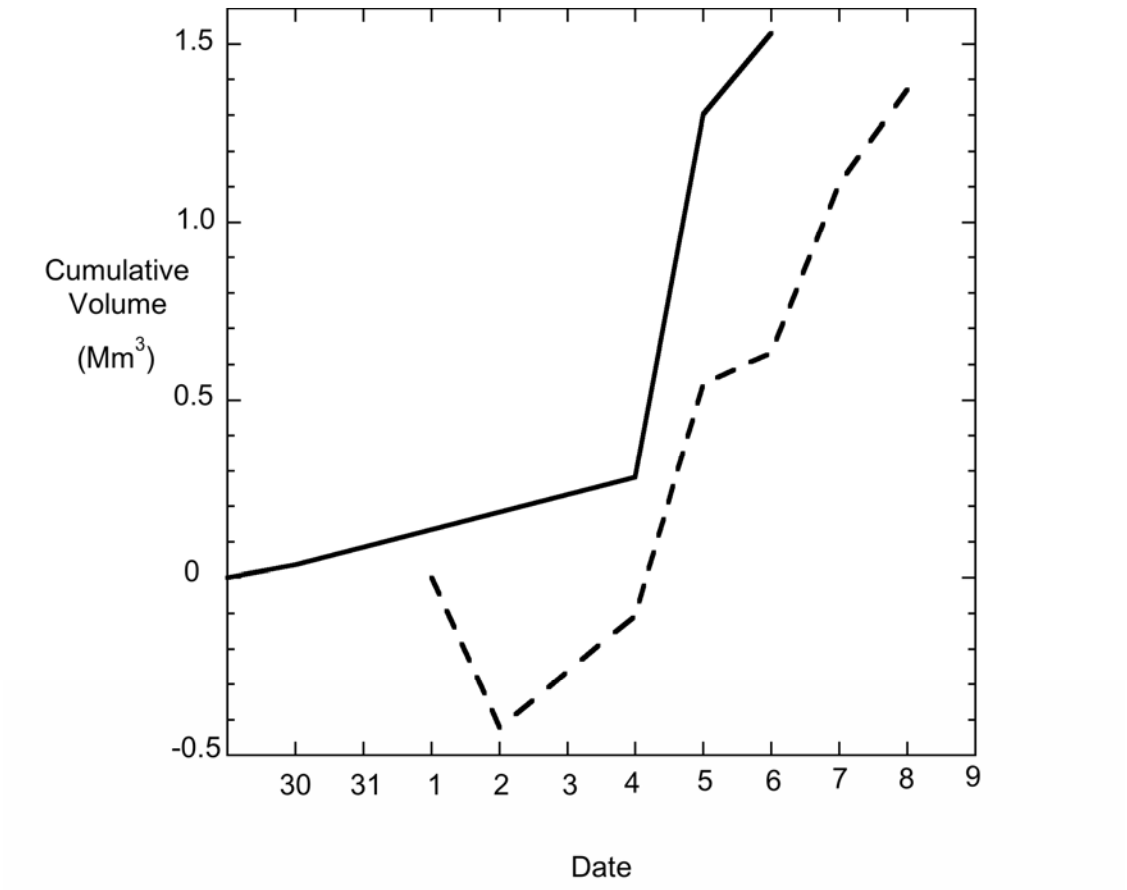

Fig. 15 Cumulative volume of lava at the summit of the dome over the period 30 March to 9 April 2006, estimated from the AVTIS intensity and range measurements made from the Runway (solid line) and Jack Boy Hill (dashed line) sites.

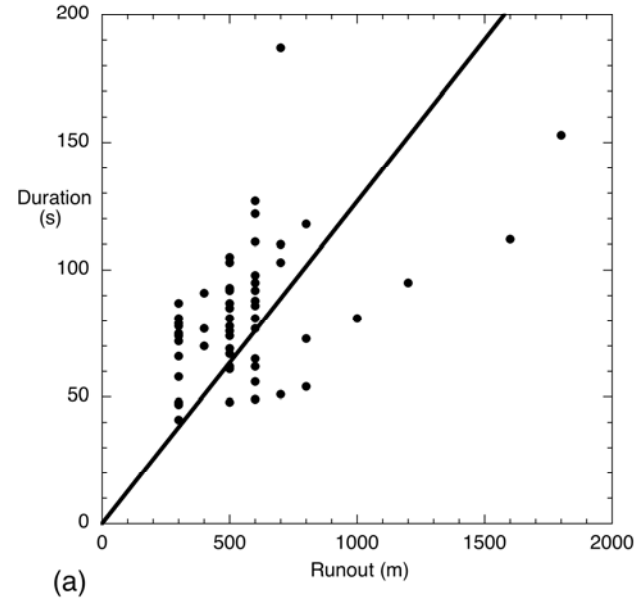

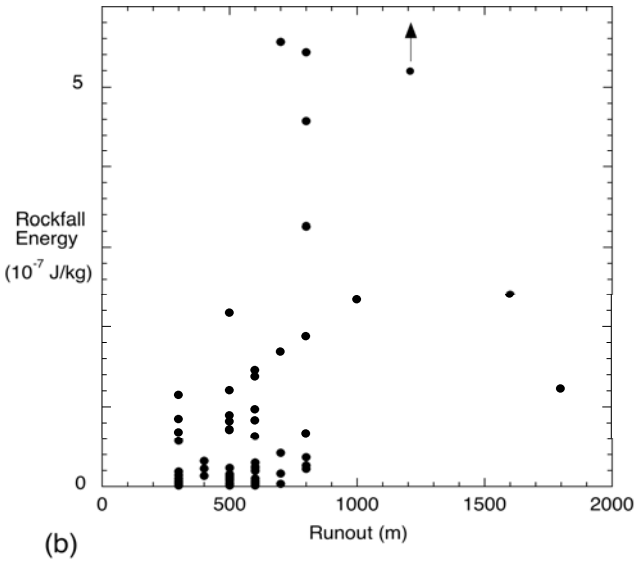

Fig. 16 Observed pyroclastic flow runout distances plotted against (a) the signal duration) recorded by the seismometer network , and (b) the energy release measured at station MBGH (arrowed event has an energy of 17.10^{-7} J/kg). The line in (a) represents a rate of 8 m/s.

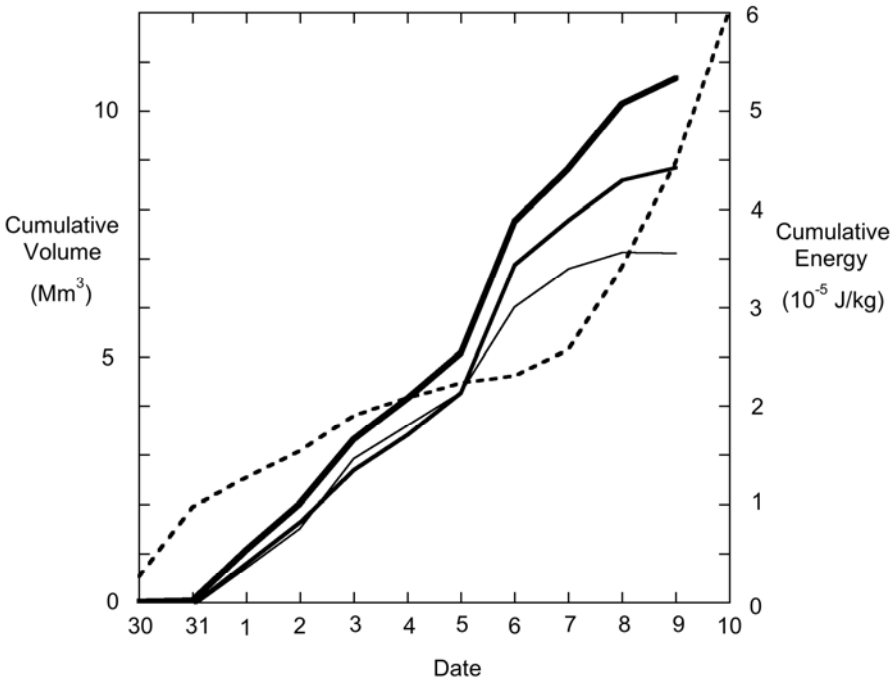

Fig. 17 Cumulative daily volumes of talus (thin solid line), talus and summit lava (medium solid line). and talus, summit lava and pyroclastic flow deposits (thick solid line). Values from Table 5. Also plotted is the cumulative seismic energy from the MBGH station.